

https://doi.org/10.1093/plcell/koae222 Advance access publication 5 August 2024 Research Article

Flavonols improve tomato pollen thermotolerance during germination and tube elongation by maintaining reactive oxygen species homeostasis

Anthony E. Postiglione, 1 Allison M. Delange, 1 Mohammad Foteh Ali, 1 Eric Y. Wang, 1 Maarten Houben, 1 Stacy L. Hahn, 1 Maleana G. Khoury, 1 Colleen M. Roark, 1 Molly Davis, 2 Robert W. Reid, 2 James B. Pease, 1, 1 Ann E. Loraine, 2 Gloria K. Muday^{1,*}

Abstract

Elevated temperatures impair pollen performance and reproductive success, resulting in lower crop yields. The tomato (Solanum lycopersicum) anthocyanin reduced (are) mutant harbors a mutation in FLAVANONE 3-HYDROXYLASE (F3H), resulting in impaired flavonol antioxidant biosynthesis. The are mutant has reduced pollen performance and seed set relative to the VF36 parental line, phenotypes that are accentuated at elevated temperatures. Transformation of are with the wild-type F3H gene, or chemical complementation with flavonols, prevented temperature-dependent reactive oxygen species (ROS) accumulation in pollen and restored the reduced viability, germination, and tube elongation of are to VF36 levels. Overexpression of F3H in VF36 prevented temperature-driven ROS increases and impaired pollen performance, revealing that flavonol biosynthesis promotes thermotolerance. Although stigmas of are had reduced flavonol and elevated ROS levels, the growth of are pollen tubes was similarly impaired in both are and VF36 pistils. RNA-seq was performed at optimal and stress temperatures in are, VF36, and the F3H overexpression line at multiple timepoints across pollen tube elongation. The number of differentially expressed genes increased over time under elevated temperatures in all genotypes, with the greatest number in are. These findings suggest potential agricultural interventions to combat the negative effects of heat-induced ROS in pollen that lead to reproductive failure.

Introduction

Global climate change has the potential to profoundly impact agriculture with increasing frequency of droughts, floods, and elevated temperatures. Global average temperatures are predicted to rise by as much as 3 °C by the end of this century (Raftery et al. 2017; Lee et al. 2019), which is sufficient to negatively impact the yield of numerous crop species. Temperature-induced reductions in crop yields of rice, wheat, com, and tomato have been shown to be as high as 30% to 50% (Sato et al. 2006; Fahad et al. 2017). Plant sexual reproduction is considered to be one of the weakest links in terms of susceptibility to increased temperature (Lohani et al. 2019). Elevated temperature can impair formation of viable pollen grains in the anthers, germination of mature pollen grains, pollen tube elongation, and fertilization of the ovules (Paupière et al. 2014; Rieu et al. 2017; Begcy et al. 2019; Raja et al. 2019; Chaturvedi et al. 2021). In tomato, heat stress impairs the development and function of pollen, with temperaturedependent effects observed at every step in this crucial process (Pressman et al. 2002; Firon et al. 2006; Sato et al. 2006; Lohani et al. 2019; Wu et al. 2020; Rutley et al. 2021). Therefore, understanding the molecular and cellular mechanisms by which elevated temperatures deleteriously affect pollen growth and development is imperative, so that innovative strategies can be developed to prevent reproductive failure.

A major plant response to heat stress in reproductive tissues is increased accumulation of reactive oxygen species (ROS) (De Storme and Geelen 2014; Muhlemann et al. 2018; Jahan et al. 2019; Torun 2019; Ali and Muday 2024; Gong et al. 2024), which may play a critical role in the observed reproductive impairments. ROS signaling is also necessary for both productive pollen tube germination and elongation, as well as coordinated tube lysis at the site of fertilization (Potocký et al. 2007; Speranza et al. 2012; Kaya et al. 2014; Jimenez-Quesada et al. 2019). However, unchecked ROS accumulation due to abiotic stresses, such as heat, can yield deleterious cellular effects including irreversible oxidative damage to nucleic acids, lipids, and proteins. Thus, oxidative stress has the ability to impact cellular processes and potentially lead to cell death (Møller et al. 2007). Although the mechanisms for synthesis of heat-dependent ROS and the biochemical targets oxidized by ROS have yet to be fully defined, the damaging effects that oxidative stress has on pollen performance are clear.

Plants employ various antioxidant mechanisms to maintain ROS homeostasis. This allows for localized ROS increases for signaling while preventing ROS accumulation from reaching damaging levels (Chapman et al. 2019; Martin et al. 2022). These include the synthesis of enzymes that detoxify ROS such as superoxide dismutases (SODs), as well as small molecules, such as glutathione, that function as cellular antioxidants (Considine and

¹Department of Biology and Center for Molecular Signaling, Wake Forest University, Winston-Salem, NC 27109, USA

²Department of Bioinformatics and Genomics, University of North Carolina, Charlotte, NC 28223, USA

^{*}Author for correspondence: muday@wfu.edu

[†]Present address: Department of Evolution, Ecology, and Organismal Biology, The Ohio State University, Columbus, OH 43210, USA.

The author responsible for distribution of materials integral to the findings presented in this article in accordance with the policy described in the Instructions for Authors (https://academic.oup.com/plcell/pages/General-Instructions) is: Gloria K. Muday (muday@wfu.edu).

Foyer 2021). Plants also synthesize several classes of specialized metabolites that contain antioxidant capacity including carotenoids, tocochromanols, and flavonoids (Chapman et al. 2019; Daryanavard et al. 2023). The flavonoid class of metabolites includes flavones, flavanone, flavonols, and anthocyanins, with flavonols and anthocyanins having the highest radical scavenging abilities (Chapman et al. 2019; Daryanavard et al. 2023). Flavonols are found in many species, and plants with mutations that alter flavonol synthesis have been shown to have impaired reproductive success in rice, corn, petunia, and tomato (Mo et al. 1992; Pollak et al. 1993; Schijlen et al. 2007; Wang et al. 2020).

Flavonol biosynthesis is conserved across the plant kingdom, although the presence, or absence, of specific metabolic sequences leads to variation in which flavonoids accumulate in different species as well as in different tissues. For example, the flavonol myricetin is synthesized in tomato (Solanum lycopersicum), and many other species, but is not synthesized in Arabidopsis thaliana (Arabidopsis) due to the absence of the gene encoding the branch point enzyme that produces this flavonol (Gayomba et al. 2017). Figure 1 illustrates the flavonol biosynthesis pathway in tomatoes, highlighting the metabolic sequence for synthesizing the 3 most abundant flavonols: kaempferol, quercetin, and myricetin.

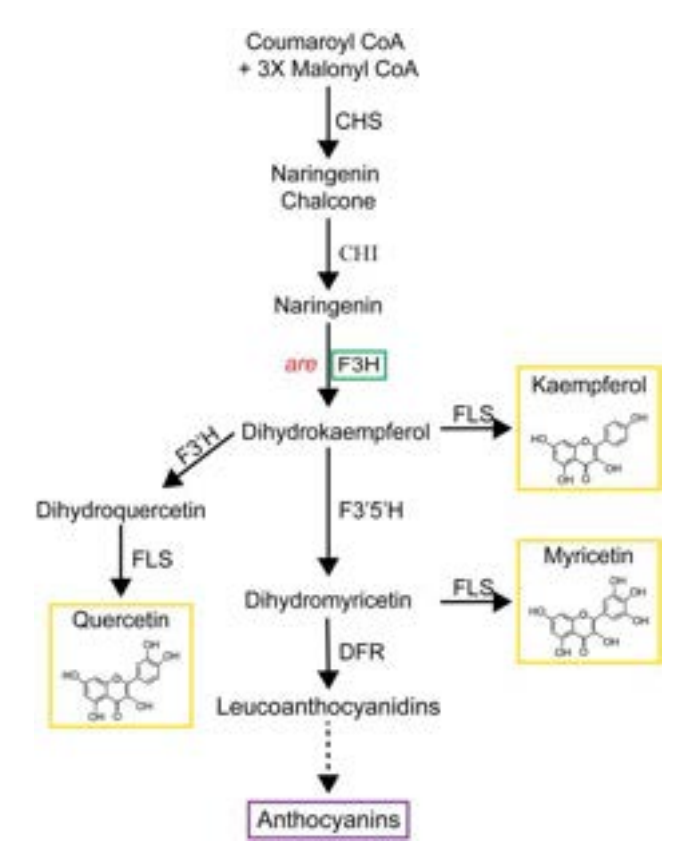


Figure 1. The flavonoid biosynthetic pathway in tomato. Pathway intermediates and enzymes that interconvert them are shown. The major intermediates of flavonoid metabolism are indicated with the enzymes catalyzing the biosynthetic reactions indicated. This paper focuses on the are mutant (in red) with a defect in the F3H enzyme, indicated in the green box. The chemical structures of the most abundant flavonols in tomato are shown within the yellow box. Enzyme abbreviations are as follows: CHS, chalcone synthase; CHI, chalcone isomerase; F3H, flavanone 3 hydroxylase, F3'H, flavonoid 3'-hydroxylase; F3'5'H, flavonoid 3'5'-hydroxylase; FLS, flavonol synthase; DFR, dihydroflavonol reductase; ANS, anthocyanin synthase. The solid lines indicate single reactions, while the dotted line indicates multiple enzymatic steps.

Additional modifications of flavonol backbones include methylation, as seen when O-methyl transferase 1 (OMT1) methylates quercetin to produce isorhamnetin, and addition of glycosyl groups to many flavonols, which produces a diverse array of distinct flavonols (Alseekh et al. 2020; Ku et al. 2020). Flavonols and anthocyanins differentially localize to distinct organs during various stages of development in tomatoes and other plants due to transcriptional regulation of pathway enzymes (Schijlen et al. 2007; Agati et al. 2012; Falcone Ferreyra et al. 2012; Pourcel et al. 2012; Groenenboom et al. 2013; Kovinich et al. 2014; Maloney et al. 2014; Gonzali and Perata 2020). For instance, anthocyanins are not synthesized in tomato pollen and roots, due to the absence of expression of genes encoding enzymes that are late in the biosynthetic pathway that lead to anthocyanin synthesis (Maloney et al. 2014; Muhlemann et al. 2018).

An important role of flavonols in pollen has also been demonstrated in tomato (Schijlen et al. 2007; Muhlemann et al. 2018; Rutley et al. 2021). Silencing the expression of the Chalcone Synthase (CHS) gene, which encodes the first enzyme of the flavonol biosynthetic pathway (see Fig. 1), resulted in parthenocarpic (or seedless) fruits (Schijlen et al. 2007). The anthocyanin reduced (are) mutant has a recessive point mutation in the single Flavanone 3-Hydroxylase (F3H) gene. This mutation causes a loss of F3H activity (Yoder et al. 1994; Maloney et al. 2014), and the mutant has been shown to have reduced levels of flavonols in roots and leaves using liquid chromatography-MS (LC-MS) (Maloney et al. 2014). This mutant also contained reduced levels of flavonols in pollen (Muhlemann et al. 2018). The are mutant has reduced pollen viability and pollen tube elongation at optimal temperatures compared to its parental line, which can be reversed by complementation with a wild-type copy of the F3H gene (Muhlemann et al. 2018). Although that work reported impaired pollen tube elongation in the are mutant at elevated temperatures, there were many unanswered questions about the impacts of temperature on other aspects of pollen performance and whether these temperature effects were tied to flavonol levels.

This work explored the impact of elevated temperatures on multiple features of pollen performance in are, a flavonoldeficient mutant, and its wild-type parental background, VF36, and these genotypes transformed with a F3H overexpression construct. These analyses revealed the negative impact of elevated temperature on pollen yield, viability, germination, tube integrity, and tube elongation, with greater impact in are than its parental line. Additionally, both genetic and chemical complementation of are reversed the temperature hypersensitivity in are and overexpression of F3H conferred thermotolerance in pollen. We visualized are pollen tube growth through VF36 and are pistils and found a reduced number of are pollen tubes in both genotypes, as compared to VF36 pollen tubes, highlighting the importance of pollen flavonols for reproductive success. Exogenous flavonols were able to protect pollen from temperature-impaired germination and tube elongation and prevent heat-dependent ROS accumulation, consistent with flavonols providing protection from temperature stress through their ROS scavenging capabilities. Additionally, the inhibition of enzymes that synthesize ROS revealed mechanisms that drive temperature stress-induced ROS. Finally, we examined the transcriptional response to elevated temperature in wild-type, the are mutant, and the transgenic line engineered to over produce flavonols across a time course of control and temperature stress treatments, to reveal genes whose expression is heat-regulated, flavonol-regulated, and associated with impaired heat stress response. This work provides insight into the mechanisms by which plants respond to heat stress, which has the potential to translate to the development of strategies to protect crops from elevated temperatures that result from our changing climate.

Results

Transformation of *are* with an F3H overexpression construct reversed pollen yield reduction and impaired viability and conveyed thermotolerance to VF36

We previously reported that the *are* mutant, which contains a point mutation in the gene encoding F3H, has a reduced pollen yield (Muhlemann et al. 2018). However, our previous study did not test whether this phenotype could be complemented with a wild-type F3H gene or investigate whether overproducing flavonols in VF36 containing this gene would increase pollen yield. To evaluate pollen yield in this mutant grown under standard greenhouse conditions, we harvested pollen from individual flowers. Pollen was resuspended in pollen viability solution (PVS), which allows pollen to hydrate without germinating. Viable pollen was then labeled with 0.4% (w/v) trypan blue in a 1:1 ratio of pollen suspension and quantified with a Countess II automated cell counter to determine the number of living grains in each flower. The ability of this method to detect live pollen is discussed in the Materials and methods section. The quantification of pollen

yield in these lines revealed that *are* had formed only 22% of the number of living pollen grains that were formed in VF36 (Fig. 2A). The *are* transformant with a Pro35S:F3H transgene (*are* Pro35S:F3H Transgenic line 5 [abbreviated *are-F3H-T5* or *are-T5*]) produced 5 times more pollen than *are*, with a yield that was not significantly different from VF36. Flowers from VF36 Pro35S:F3H Transgenic line 3 (VF36-F3H-T3 or VF36-T3) contained 2-fold greater yield of viable pollen grains as compared to VF36 flowers and 9.1-fold greater yield than *are* (Fig. 2A).

The viability of pollen at optimal and elevated temperatures was also examined in these 4 lines. Previously, we showed that growth of tomato plants under several days of temperature stress reduced the viability of are pollen more than VF36 (Muhlemann et al. 2018), but we did not examine the effect of short-term hightemperature treatments on viability of pollen grains. Pollen samples were collected from plants grown under optimal conditions and incubated in PVS at 28 °C (optimal temperature) or 34 °C (heat stress) for 2 h. At the end of this incubation, pollen grains were costained with 0.001% fluorescein diacetate (FDA) (w/v) and 10 µm propidium iodide (PI) to mark viable and nonviable grains, respectively (Fig. 2B). Imaging with a laser scanning confocal microscope (LSCM) revealed that 70% of the VF36 grains were viable after exposure to optimal temperatures, while only 29% of are grains were viable (Fig. 2C). When pollen from each genotype was exposed to temperature stress (34 °C for 2 h), viability fell to

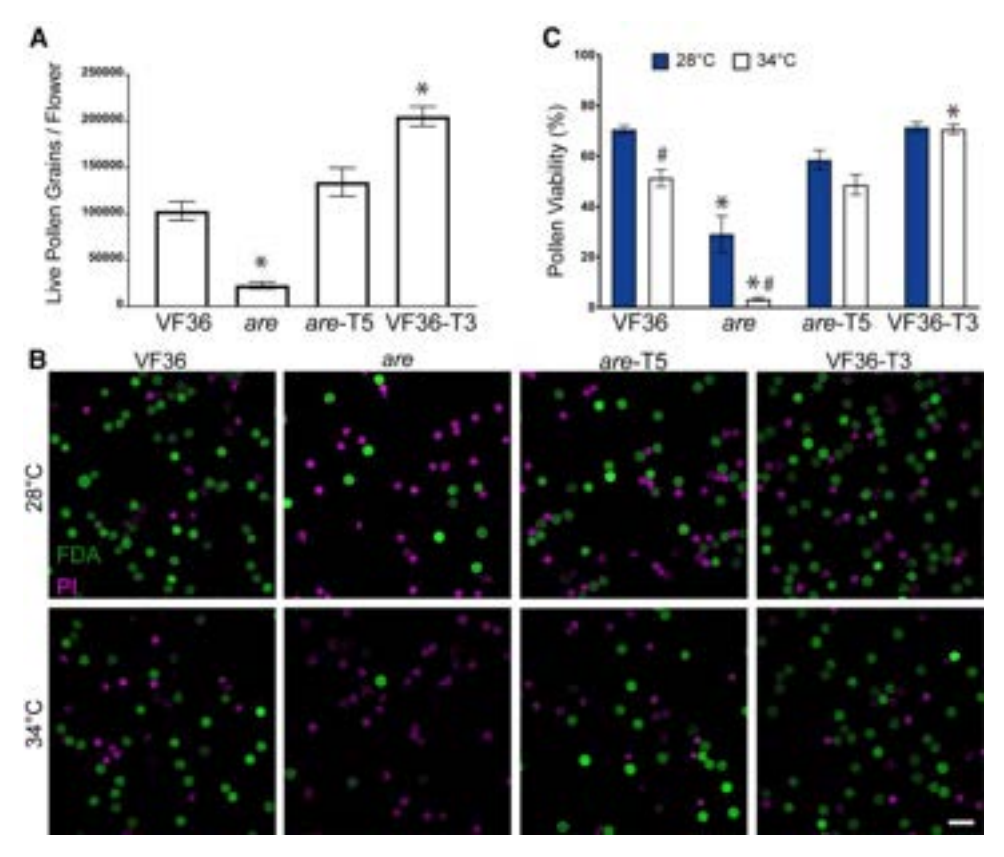


Figure 2. Flavonols positively regulate pollen yield and protect pollen viability during heat stress. A) Quantification of the average number of live pollen grains per flower ± SEM in each genotype immediately upon harvesting. Three independent replicates were quantified with each replicate containing 4 flowers per genotype. B) Representative confocal micrographs of pollen grains of VF36, are, are complemented with a Pro35S:F3H transgene (are-T5), and VF36 transformed with this same transgene (VF36-T3). Pollen grains incubated at either 28 or 34 °C for 2 h and then costained with FDA (denoting live grains in green) and PI (denoting dead grains in magenta). Scale bar: 50 μm for all panels. C) Quantification of the percentage of viable pollen grains of VF36, are, are-T5, and VF36-T3 after 2-h incubation at 28 or 34 °C from 4 independent experiments with > 850 pollen grains for each sample. Error bars represent sr of the mean. Asterisks denote significant differences from VF36 at the same temperature, and hash marks denote significant differences between temperatures within the same genotype according to a 2-way ANOVA followed by a Tukey post hoc test with a P < 0.05.

51% for VF36, with only 3.5% viability of are pollen grains. The are-F3H-T5 line had significantly greater pollen viability than the are mutant, at levels equivalent to VF36 at both optimal and elevated temperatures (Fig. 2, B and C). The VF36-F3H-T3 transgenic line had similar percentages of viable pollen as VF36 at optimal temperatures, but when pollen was treated for 2 h at 34 °C, the VF36-F3H-T3 line showed no reductions in pollen viability at this elevated temperature (Fig. 2, B and C), consistent with this gene conferring thermotolerance. We also examined viability in pollen directly after hydration in PVS using the same staining methods (Supplementary Fig. S1). The percent viability of these pollen grains was similar to those hydrated for 2 h, consistent with PVS incubation at optimal temperatures not affecting pollen viability over a 2-h time course.

Lines transformed with an F3H overexpression construct have increased F3H expression and flavonol levels in anther tissue and increased flavonol accumulation in pollen tubes

Multiple transgenic lines of are and VF36 lines transformed with a Pro35S:F3H gene were previously shown to have increased flavonol accumulation in roots and leaves in comparison to the untransformed lines and similar root developmental phenotypes (Maloney et al. 2014), though flavonol accumulation was not quantified in reproductive tissues. The plants used in these experiments have F3H driven by the 35S promoter because these transformants were originally made to examine the effect of this F3H gene in vegetative tissues (Maloney et al. 2014). There is conflicting evidence in the literature on whether the 35S promoter is expressed in pollen (Eyal et al. 1995; Sunilkumar et al. 2002; de Mesa et al. 2004; Koul et al. 2012), which we elaborate upon in the Materials and Methods section. Additionally, published evidence suggests that flavonol accumulation in pollen is deposited during pollen development by tapetum cells within the anther (van Eldik et al. 1997; Shi et al. 2021; Xue et al. 2023); therefore, we evaluated F3H expression in anther tissue of VF36 and VF36-F3H-T3. Using reverse transcription quantitative PCR (RT-qPCR) of anther samples, we found 1.5-fold higher levels of F3H transcript in VF36-F3H-T3 than in VF36, consistent with elevated transcript synthesis in anthers driven by the 35S promoter (Supplementary Fig. S2).

We also extracted flavonols from anthers and isolated pollen of all 4 genotypes. Anthers from are contain 21-fold more naringenin (the F3H substrate) than either VF36 or the genotypes transformed with this construct (Supplementary Table S1). The are pollen had 16-fold more naringenin than VF36. The are anthers and pollen also had significant reductions in the flavonol kaempferol relative to VF36 (1.4- and 1.6-fold, respectively), which is downstream of the nonfunctional F3H enzyme in are (Fig. 1) and has previously been shown to be an important metabolite in pollen growth (Mo et al. 1992; Pollak et al. 1993). In the are-T5 line, both the increased naringenin and reduced kaempferol were reversed in pollen and anthers, resulting in levels of naringenin and kaempferol not being significantly different from VF36. Additionally, VF36-T3 anthers contained significantly increased kaempferol levels, which were 1.4-fold higher than VF36 (Supplementary Table S1). In contrast, this construct did not lead to significant detectable increases in kaempferol in pollen (Supplementary Table S1). These results parallel the change in F3H levels in VF36 due to the presence of Pro35S: F3H transgene, which are more profound in anthers than in pollen.

To verify that levels of flavonol synthesis in anthers resulted in the expected differences in flavonol levels within pollen tubes, and to determine the distribution of flavonols in pollen tubes, we visualized flavonols via the fluorescent chemical probe diphenylboric acid 2-aminoethyl ester (DPBA). Pollen from each genotype was hydrated in pollen germination medium (PGM) and incubated at 28 °C for 60 min to allow for pollen tube elongation. Pollen was then labeled with DPBA for 30 min and imaged under high magnification, and flavonol distribution was quantified in the region $40\,\mu m$ from the pollen tip. Representative images of pollen tubes are shown in Fig. 3A, and DPBA fluorescence was quantified with a line profile from the tip of the pollen tube back (Fig. 3B). The DPBA fluorescence shows an interesting distribution along the pollen tube. The signal is low at the pollen tube tip (in the clear zone that is the 7 µm closest to the tip), and the signal increases as the distance from the tip increases. Flavonol levels were significantly reduced by 1.6-fold in are pollen tubes when the average of the line was compared to VF36 tubes. Both are-T5 and VF36-T3 showed significant increases in flavonol accumulation relative to the parental lines, with VF36-T3 displaying the highest flavonol levels.

In are, pollen germination and tube elongation are hypersensitive to elevated temperatures and this effect is reversed by a wild-type F3H gene

The effect of temperature stress on pollen germination had not been examined previously in either are and VF36, or the lines transformed with our Pro35S:F3H construct. Therefore, we asked whether impaired pollen germination under temperature stress was also accentuated in are and reversible by the Pro35S:F3H gene. Pollen from all 4 genotypes was hydrated in PGM for 30 min at either 28 or 34 °C, and images were captured using an inverted light microscope. Representative images of pollen grains from are, VF36, are-T5, and VF36-T3 are shown in Fig. 4A, revealing many ungerminated pollen grains and pollen grains or tubes that had burst. The percentage of live pollen grains that germinated was quantified in Fig. 4B, using criteria defined and elaborated in the Materials and methods section. Only 61% of are pollen grains germinated at optimal temperature relative to the other 3 genotypes that have ~80% germination. The impaired germination of are is accentuated at elevated temperature, where germination is reduced to 44%. In contrast, both the are-T5 and VF36-T3 lines have similar germination rates to VF36 at optimal temperature, but significantly greater germination than VF36 at elevated temperatures, suggesting that engineering plants to increase flavonol levels can enhance thermotolerance during pollen germination.

To verify that these effects were linked to the elevated expression of the F3H gene, we quantified germination in an additional Pro35S:F3H transformant for each of the are and VF36 genotypes (Supplementary Fig. S3), which were part of a larger set of transgenics that were shown to have altered flavonoid metabolites and root developmental defects (Maloney et al. 2014). These transgenics lines have similar ability to reverse the poor germination in are and convey thermotolerance to VF36. These findings are consistent with a model that the impaired pollen germination in are is linked to the F3H mutation and flavonols synthesized by a 35S promoter-driven F3H gene are sufficient to complement the mutant temperature hypersensitivity phenotype. In both VF36-T3 and VF36-T5 lines, we observed no reductions in germination at the higher temperature, consistent with these lines being resistant to the negative effects of elevated temperature on pollen germination (Fig. 4B, Supplementary Fig. S3).

We had previously reported that elevated temperatures impaired pollen tube elongation in the are mutant relative to optimal temperature and to the VF36 parental line (Muhlemann et al.

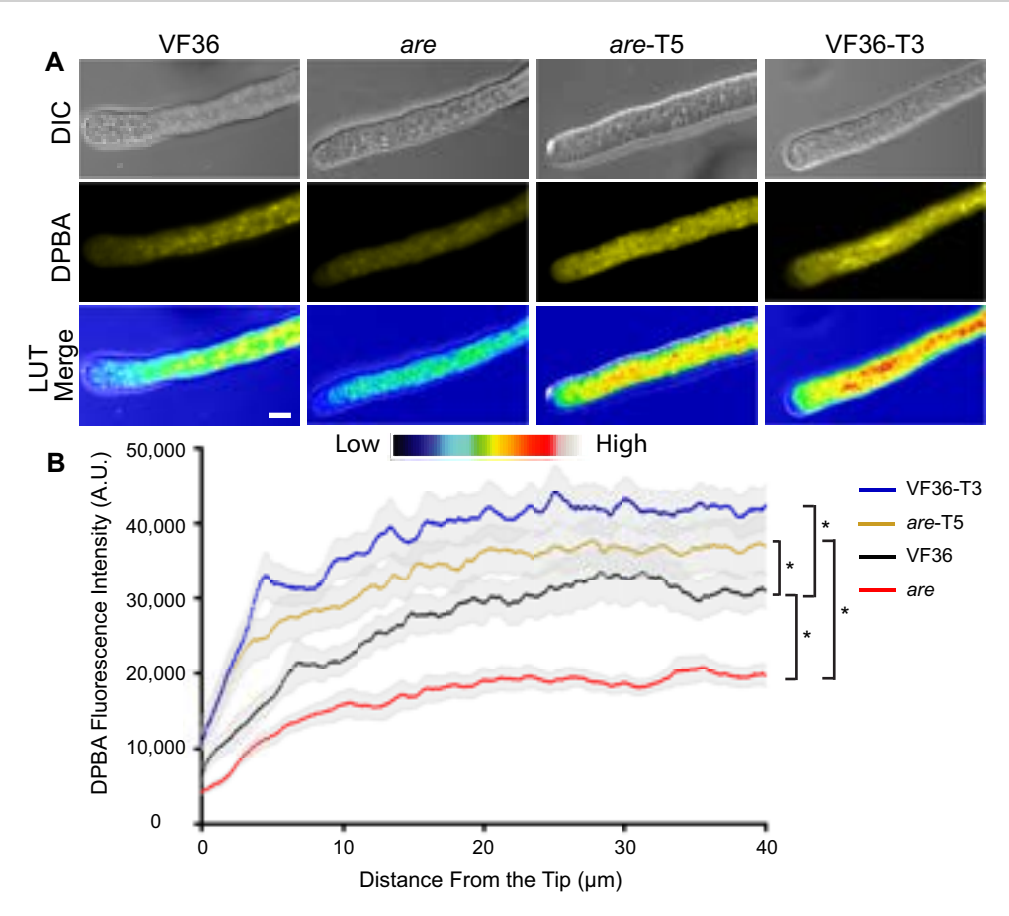


Figure 3. Flavonols are present in the pollen tube at greater magnitudes in tomato lines with a functional F3H gene. A) Representative confocal micrographs of flavonol levels in VF36-are, are-T5, and VF36-T3 pollen tubes as visualized by DPBA staining. DPBA fluorescence is shown in yellow as well as converted to a LUT scale with the indicated scale. Size bar: 10 µm for all images. B) Quantification of the DPBA fluorescence intensity across a 50-pixel wide, 40 µm long line profile beginning at the pollen tube tip. The average of 3 independent experiments was quantified with each replicate containing 5 tubes per genotype with the gray shading denoting the SE of the mean. Asterisks denote significant differences between genotypes indicated by brackets according to a 1-way ANOVA followed by a Tukey post hoc test with a P < 0.05.

2018). We asked whether temperature-impaired pollen tube elongation in *are* could be reversed with a wild-type copy of the F3H gene and abolished when the 35S promoter-driven F3H gene is in the VF36 background. Pollen from the same 4 genotypes (VF36, *are*, *are*-T5, and VF36-T3) was hydrated in PGM before incubation at 28 °C for 30 min to germinate pollen tubes. Half the samples from each genotype remained at 28 °C for 90 min to allow pollen tube elongation and half were then transferred to 34 °C for 90 min. Pollen tubes were then imaged via brightfield microscopy and tube length was measured.

At optimal temperatures, VF36 pollen tubes elongated 1.3-fold more than *are* pollen tubes after the 2-h time course (Fig. 4, C and D). Pollen tube length was significantly greater in *are*-F3H-T5 when compared to *are* with lengths not significantly different from VF36 (Fig. 4D). We also observed that VF36-F3H-T3 pollen tubes were significantly longer than VF36 following incubation at optimal temperatures, consistent with elevated flavonols protecting pollen tube growth from temperature stress.

Heat treatment significantly reduced pollen tube length in VF36 and *are*, relative to optimal temperature, with heat stressed *are* pollen having the shortest pollen tubes (Fig. 4D). Tube extension at elevated temperatures was still decreased in the *are-F3H-T5* line, though tube length was not significantly different than VF36 at this temperature. Additionally, pollen tube length in VF36-F3H-T3 was not significantly impaired by exposure to heat stress (Fig. 4D). These data are consistent with the

thermotolerance of pollen being dependent on the levels of flavonols, with reduced pollen tube length in *are* and VF36, while the *are*-T5 and the VF36-T3 transgenic lines displayed enhanced pollen tube elongation, especially under elevated temperature.

Pollen tube rupture is more prevalent in are at both temperatures and is not rescued via coincubation with VF36 pollen

We had previously reported that pollen tubes rupture at greater levels in are relative to VF36 at optimal temperatures (Muhlemann et al. 2018), but we had not examined the effect of elevated temperature on this response or how this response was affected in the F3H transgenic lines. To assess the impact of the are mutation on this process, we simultaneously measured pollen tube rupture in are and VF36 in the same wells. To make this simultaneous analysis possible, we utilized a GFP construct driven by the pollen-specific promoter, ProLAT52, that was originally transformed into the VF36 background (Zhang et al. 2008) and that we crossed into are. This allowed for pollen from VF36 ProLAT52:GFP and untransformed are to be incubated together and tube rupture to be quantified for both samples simultaneously. We also performed the reciprocal experiment with are ProLAT52:GFP incubated with untransformed VF36 pollen. Pollen tubes were elongated as described previously and the percentage of ruptured pollen tubes was quantified at both optimal and

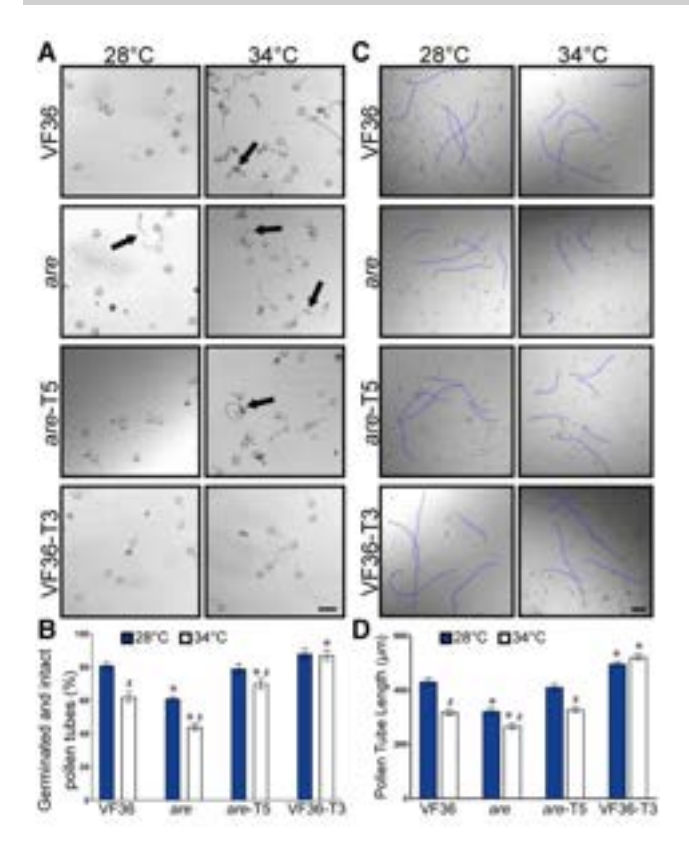


Figure 4. The negative effects of high temperature on tomato pollen germination and tube length are accentuated in are and reversed by an F3H transgene. A) Representative brightfield images of VF36, are, are-F3H-T5, and VF36-F3H-T3 pollen germination after 30 min at either 28 or 34 °C. Arrows denote ruptured pollen. Scale bar: 50 µm in all panels. B) Quantification of percent pollen germination that exhibited intact tubes after 30 min and the average and SE of the mean from 3 independent experiments (n > 90 pollen grains per genotype and treatment). C) Representative images of pollen tubes elongating for 120 min at 28 °C, or at 30 min at 28 °C, and then transferred to 34 °C for an additional 90 min. Five pollen tubes from each image are highlighted in blue to enhance visibility. Scale bar: 100 µm in all panels. D) Quantification of mean pollen tube length is shown for >200 pollen tubes per genotype and treatment. Error bars represent SE of the mean. B and D) Asterisks denote significant differences from VF36 at the corresponding temperature, and hash marks denote significant differences between temperatures within the same genotype according to a 2-way ANOVA followed by a Tukey post hoc test with a P < 0.05.

elevated temperatures. Incubation at 34 °C significantly increased rates of ruptured pollen tubes in both lines, though pollen tubes from VF36 ProLAT52:GFP showed significantly lower rates of rupture when compared to are at both temperatures (Fig. 5, A and B). Coincubation of are ProLAT52:GFP with VF36 pollen also showed higher rates of rupture in the are background regardless of temperature, suggesting that the reduced levels of flavonols in are lead to greater pollen tube bursting during elongation than in VF36 (Fig. 5, C and D).

ROS levels in pollen grains and tubes are inversely proportional to levels of flavonol antioxidants and are increased at elevated temperature

To determine whether the protective effect of flavonols on pollen performance was due to their ROS scavenging activity in the pollen interior, we monitored ROS accumulation during the pollen germination and pollen tube elongation phases in VF36, are, are-F3H-T5, and VF36-F3H-T3 lines. We used 2'-7'-dichlorodihydrofluorescein

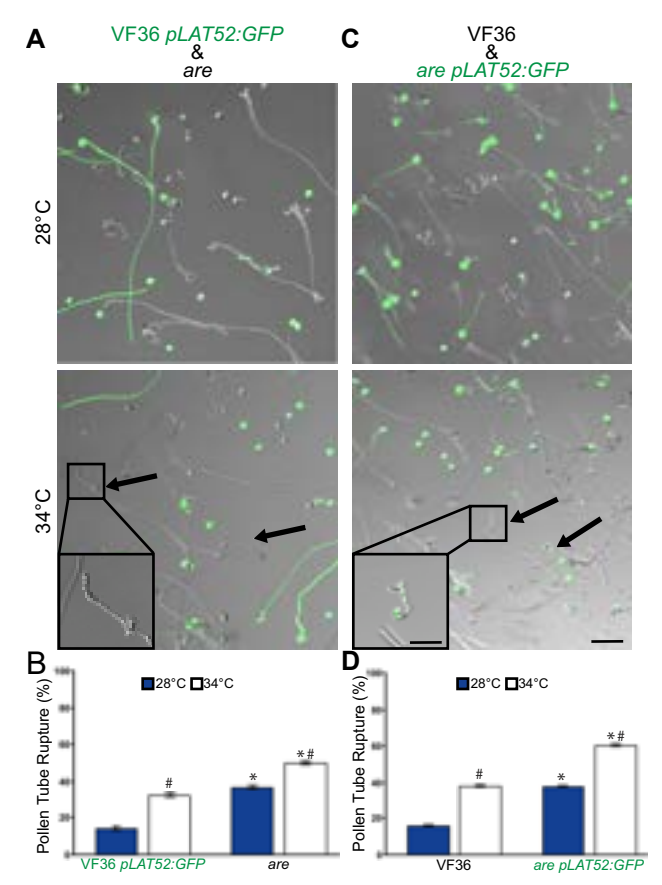


Figure 5. The heat accentuated rupturing of are pollen tubes is not improved by culturing with the VF36 parental line. A) Representative images of pollen tubes of VF36 ProLAT52:GFP (green) germinated along with untransformed are. Pollen was germinated in vitro and for 120 min at 28 °C or for 30 min at 28 °C followed by 90 min at 34 °C. B) Quantification of mean percent pollen tube rupture for VF36 ProLAT52:GFP and are (n > 500 pollen grains for each genotype from 3biological replicates with 6 technical replicates within each sample). Error bars represent se of the mean. C) Representative images of pollen tubes of VF36 germinated with are ProLAT52:GFP (green). D) Mean percent pollen tube rupture ± SEM for VF36 and are ProLAT52:GFP (n > 500 pollen grains for each genotype from 3 biological replicates)with 6 technical replicates within each sample). A and C) Scale bar: 100 µm in both panels. Arrows denote ruptured pollen in are. Square insets show a magnified view of ruptured pollen tubes with a 40 μm scale bar in both inserts. Asterisks denote significant differences between genotype at the same temperature, and hash marks denote significant differences between temperatures within the same genotype according to a 2-way ANOVA followed by a Tukey post hoc test with a P < 0.05.

diacetate (CM-H₂DCFDA, DCF), a chemical probe that can be oxidized by multiple ROS species, to quantify the relative levels of ROS accumulation in germinating pollen grains and elongating pollen tubes in these 4 genotypes under optimal and elevated temperatures.

ROS accumulation was examined during germination, and pollen grains were hydrated in PGM at 28 or 34 °C for 10 min and then further incubated in PGM containing CM-H2DCFDA for an additional 20 min at the same temperatures to monitor ROS levels during the early stages of germination. The fluorescence intensity of pollen grains was then examined with a Zeiss 880 LSCM (Fig. 6A), and these values are reported as a LUT, which makes the brighter fluorescence in are pollen easier to visualize. DCF fluorescence in mature, viable grains was then quantified and normalized to fluorescence intensity of VF36 at 28 °C. At 28 °C, pollen grains from the are mutant had a significant 1.4-fold higher DCF fluorescence

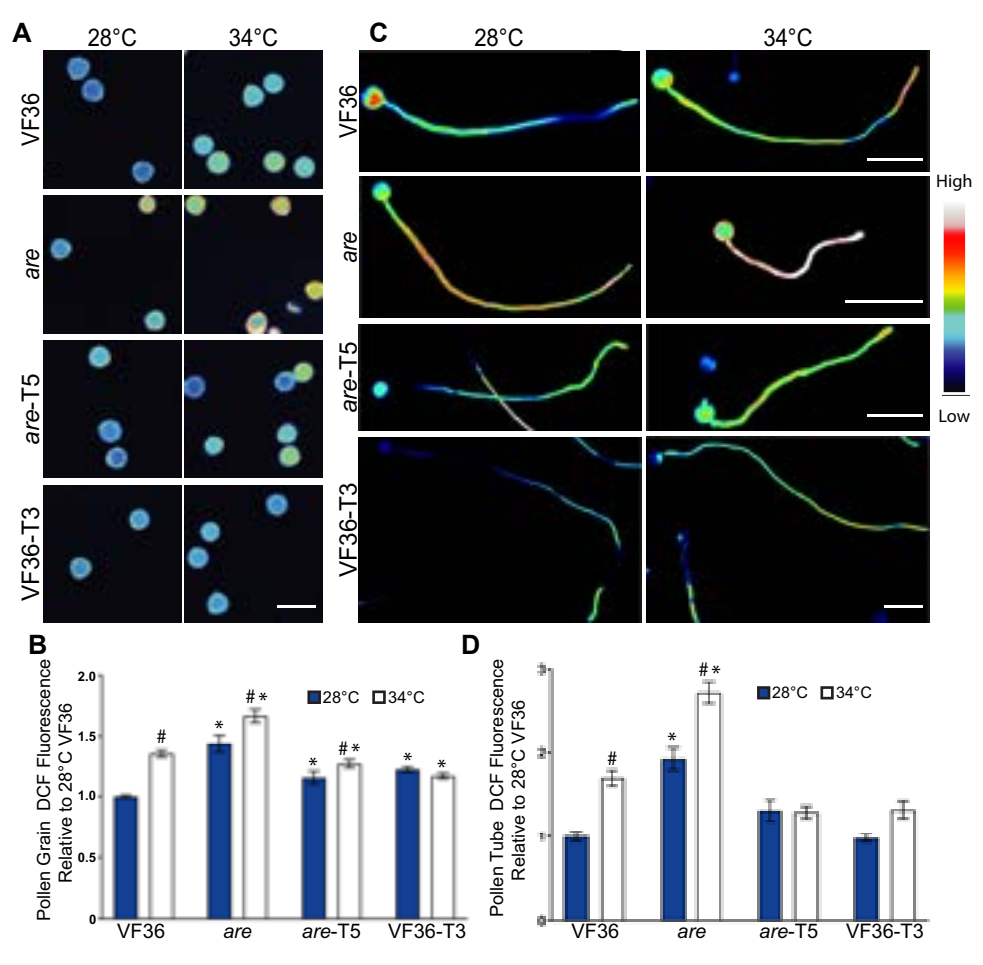


Figure 6. Heat-induced ROS accumulation in germinating pollen grains and elongating pollen tubes is reduced with increased flavonol synthesis. A) Representative confocal micrographs of pollen grains germinated for 10 min and then stained with CM- H_2 DCFDA for 20 min. DCF fluorescence has been converted to a LUT scale for visualization with the range shown in the color scale. Scale bar: 50 μ m for all panels. B) The mean and se of fluorescence of germinating pollen relative to VF36 at 28 °C across 4 to 5 independent experiments are reported (n > 89 grains per genotype and treatment). C) Representative fluorescent images of pollen tubes germinated for 30 min at 28 °C and then transferred to 28 or 34 °C for an additional 90 min. Pollen tubes were then stained with CM- H_2 DCFDA for 20 min. DCF fluorescence has been converted to a LUT scale for visualization with the range shown as a color scale. The VF36-T3 images are zoomed out as these pollen tubes are longer. Scale bars: 100 μ m for all pollen tube images. D) The mean fluorescence of elongating pollen tubes relative to VF36 at 28 °C across 3 independent experiments is reported with the error bars representing the se of the mean (n > 85 tubes per genotype and treatment). Fluorescence values were normalized to the VF36 pollen germinated at 28 °C. Asterisks denote significant differences from VF36 at the same temperature, and hash marks denote significant differences between temperatures within the same genotype according to a 2-way ANOVA followed by a Tukey post hoc test with a P < 0.05.

than VF36 (Fig. 6B). At 34 °C, both genotypes exhibited significantly higher ROS levels relative to VF36 at 28 °C. Heat stressed VF36 and are showed 1.4-fold and 1.7-fold higher fluorescence than at 28 °C, respectively. The are transgenic line, are-F3H-T5, exhibited a significant 1.2-fold reduction in DCF relative to are at 28 °C. are-T5 also had significantly reduced DCF fluorescence at 34 °C relative to are at 34 °C. The DCF fluorescence in pollen grains of the VF36-T3 line was not increased by elevated temperatures, with similar fluorescence at both 28 and 34 °C, consistent with enhanced thermotolerance and the absence of response to this acute heat stress (Fig. 6B).

To evaluate ROS accumulation in elongating pollen tubes, pollen grains were allowed to germinate for 30 min at 28 °C and then transferred to elevated temperature stress of 34 °C for 90 min, while control samples remained at 28 °C for the additional 90-min period. Pollen tubes were then labeled with CM-H₂DCFDA for an additional 20 min and imaged as described above (Fig. 6C). This signal is bright throughout most of the tube, and the swollen tube tip in are at 34 °C is consistent with a tube that is close to rupturing. Pollen tube

length of *are* is shorter, especially at elevated temperatures, while VF36-T3 pollen tubes are longer than other genotypes, consistent with observations of pollen tube length in Fig. 4, C and D. DCF fluorescence was quantified in these pollen tubes revealing that heat stress significantly increased ROS accumulation in VF36 and *are* relative to VF36 at 28 °C by 1.8- and 2.7-fold, respectively (Fig. 6D).

To gain more detailed insight into the type of ROS increased with elevated temperature and the distribution of this ROS in pollen tubes, we also labeled pollen tubes with the hydrogen peroxide (H_2O_2) selective probe, Peroxy Orange 1 (PO1). Consistent with our DCF results, heat stress significantly increased PO1 intensity in both VF36 and *are*, with the most substantial increase observed in *are* (Fig. 7). The levels of H_2O_2 in *are*-T5 and VF36-T3 were unaffected by elevated temperatures, consistent with flavonol antioxidants conveying thermotolerance via maintaining ROS homeostasis. PO1 fluorescence was at the highest levels at the tip of the pollen tube, especially in VF36 and *are* which showed slightly increased H_2O_2 within this region. This is consistent with the lowest levels of flavonol antioxidants at the pollen tube tip in these 2

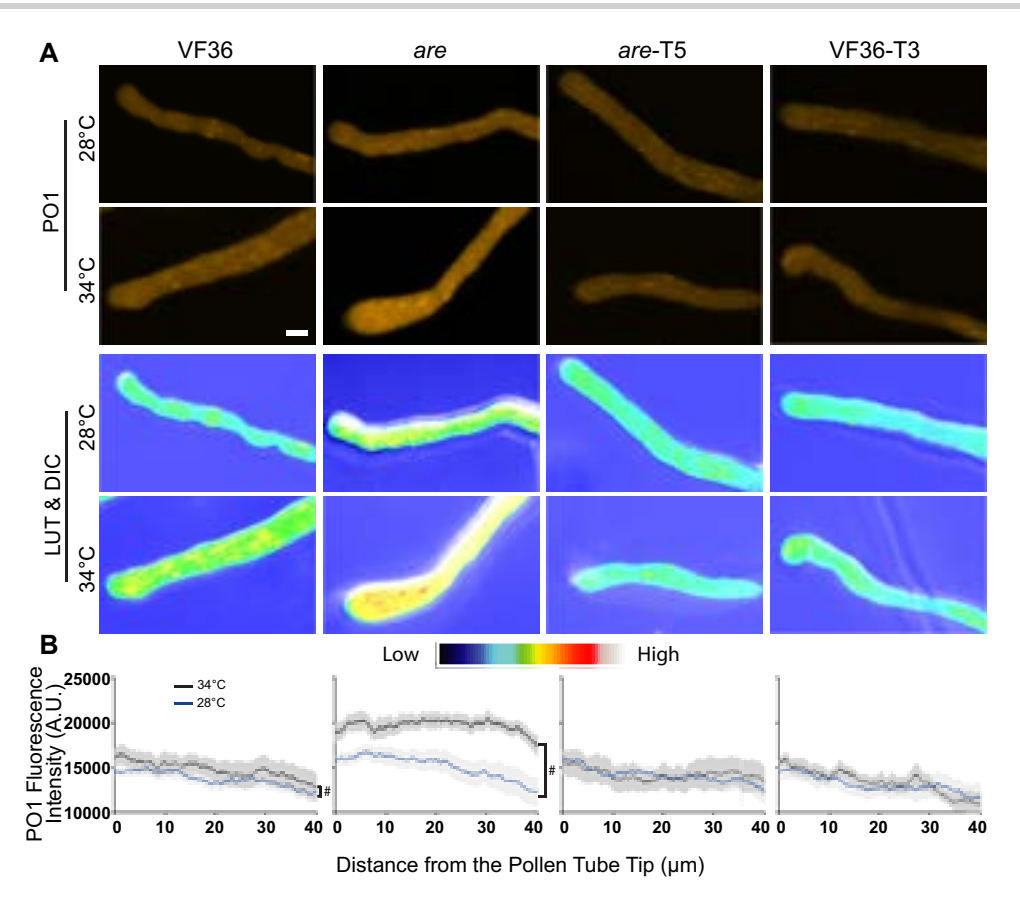


Figure 7. Elevated temperature increases H₂O₂ accumulation in VF36, and are pollen tubes, but not are-T5 nor VF36-T3. A) Representative confocal micrographs of PO1 fluorescence in VF36-are, are-T5, and VF36-T3 pollen tubes germinated for 30 min at 28 °C and then transferred to 28 °C (blue line) or 34 °C (black line) for an additional 90 min. PO1 signal intensity is converted to a LUT scale with the relative range of intensity shown in the color scale. Scale bar: 10 µm. B) Quantification of the PO1 fluorescence intensity across a 50-pixel wide, 40 µm long line profile beginning at the pollen tube tip. Three independent experiments were quantified with each replicate containing 5 tubes per genotype, and the blue represents fluorescence in 28 °C samples and the black line in 34 °C samples. The average is graphed with the gray shading representing the sE of the mean. The hash symbols denote significant differences between 28 and 34 °C within the same genotype according to a one-way ANOVA followed by a Tukey post hoc test with a P < 0.05.

genotypes. The magnitude difference in PO1 signal between genotypes is less than for DCF, which may be consistent with multiple ROS changing in response to elevated temperature or could reflect difference in the chemistry of PO1, which is less sensitive than other dyes or biosensors (Martin et al. 2022).

The substantially higher levels of PO1 and DCF signal in are pollen tubes, especially at 34 °C, are consistent with elevated ROS leading to reduced pollen tube length at elevated temperature. These results indicate that increased flavonol synthesis maintains ROS homeostasis at elevated temperatures, and high-temperature-driven ROS accumulation in elongating pollen tubes was observed in both VF36 and are but was absent in are-F3H-T5 and VF36-F3H-T3 (Figs. 6D and 7). These results are consistent with elevated ROS in a mutant impaired in synthesis of flavonol antioxidants. This finding also sheds light on the mechanism for the enhanced thermotolerance of the are-F3H-T5 and VF36-F3H-T3 lines as temperature-induced ROS increases can be mitigated through increased production of flavonol antioxidants.

Exogenous flavonols reduce the effect of heat stress on germination and tube length of VF36 and are pollen

The data described above reveal the positive effect of endogenously synthesized flavonols on maintaining ROS homeostasis, improved pollen yield, viability, germination, and tube growth, especially under high-temperature stress. However, these data do not reveal which flavonols have this effect, at what stage flavonols function, and whether exogenous flavonols can be taken up by pollen to reverse the are phenotypes. To further demonstrate that the impaired germination in the are mutant is tied to reduced flavonol levels, and to ask whether specific flavonols confer protection to pollen, we performed chemical complementation of are using exogenous flavonols.

We utilized the flavonols kaempferol, quercetin, and myricetin, whose synthesis occurs in the biosynthetic pathway after the F3H enzyme, which is nonfunctional in are (Fig. 1). We harvested pollen grains and placed them in PGM containing solvent or flavonols at doses of 5 and 30 μ M and assessed germination after 30 min at 28 or 34 °C (Fig. 8A). Chemical supplementation with 5 μM kaempferol reversed the impaired pollen germination in are at 28 °C to levels equivalent to VF36. Kaempferol also significantly improved the germination of are pollen at 34 °C. Additionally, kaempferol was also able to protect VF36 from temperature-impaired germination with VF36 germination at 34 °C significantly increased with treatment with either 5 or 30 μm kaempferol from 62% in untreated controls to 80%. We also examined the effect of treatment with similar doses of quercetin and myricetin and found that both of these flavonols also restored germination in are to wild-type levels and reduced the effect of elevated temperatures in both VF36 and are (Supplementary Fig. S4). The findings that even pollen grains detached from the flower are still protected from heat

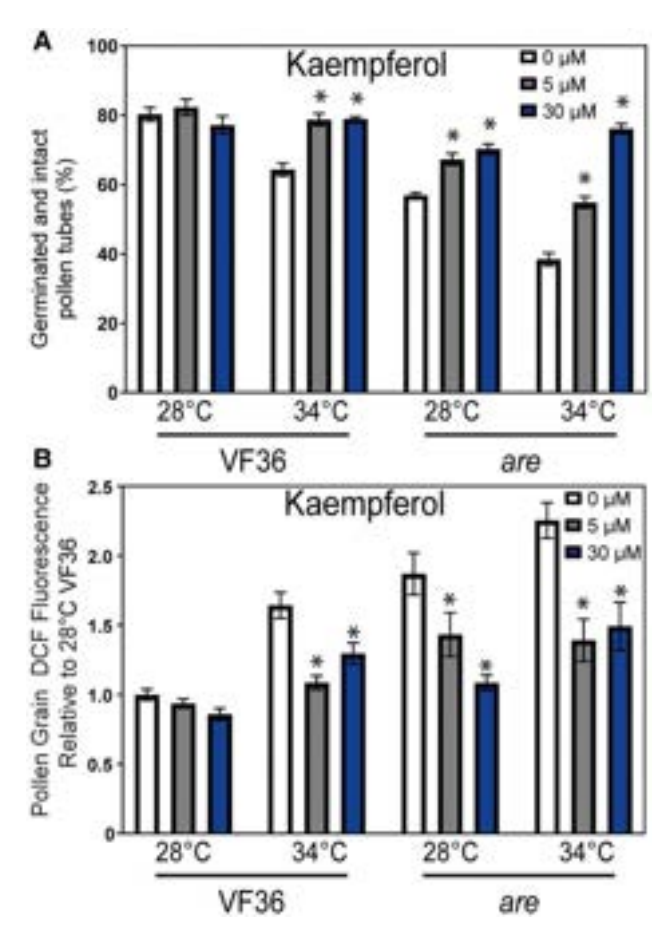


Figure 8. Impaired pollen germination in are is reversed by supplementation with the flavonol kaempferol. A) The percentage of VF36 and are pollen grains that germinate with and without exogenous kaempferol treatment was examined at doses of 0, 5, or 30 μ M at 28 or 34 °C. The mean and se are reported for percent germination in the presence and absence of flavonols were determined in 3 to 4 independent experiments with n>80 grains per sample. B) The mean and se of fluorescence intensity of DCF in germinating pollen grains incubated with 0, 5, or 30 μ M kaempferol are reported relative to VF36 at 28 °C across 4 independent experiments (n>40 grains per genotype and treatment). A and B) Asterisks denote significant differences from 0 μ M flavonol treatment within genotype and temperature treatment according to a 2-way ANOVA followed by a Tukey post hoc test with a P<0.05.

stress by flavonols suggest that flavonols function specifically within pollen grains and that all 3 flavonols can protect mature pollen from high-temperature stress. This broad action of all 3 flavonols differs from other cases where specific flavonols have unique functions, such as in the control of root hair and lateral root formation in Arabidopsis (Gayomba and Muday 2020; Chapman and Muday 2021).

We examined the ability of exogenous flavonols to enter pollen and scavenge ROS within the grains by incubating are and VF36 in PGM supplemented with kaempferol at 0, 5, or 30 $\mu \rm M$ at optimal and elevated temperatures and visualized ROS in pollen grains with CM-H2DCFDA as described above. Treatment with exogenous kaempferol did not alter DCF levels in VF36 grains at either concentration at 28 °C, though both concentrations were able to significantly decrease DCF levels in are at this temperature when compared to untreated controls (Fig. 8B). In pollen germinated at 34 °C, kaempferol at both 5 and 30 $\mu \rm M$ was also able to diminish the elevated DCF intensity in both VF36 and are pollen grains.

The are stigma has reduced flavonol levels and elevated H_2O_2 levels

We asked whether levels of flavonol antioxidants and ROS were altered in stigmas of are and VF36 to gain an understanding of how this mutation affected redox balance in female reproductive organs. VF36 and are pistils were stained with DPBA to detect flavonols and the resulting representative epifluorescence micrographs of the stigmas are shown in Fig. 9A. Quantification of DPBA fluorescence intensity of these images is reported relative to VF36 revealing a 2-fold reduction in signal in the are pistils (Fig. 9B). This result is consistent with the reduced flavonol levels in pollen, roots, and leaf tissues of this mutant (Maloney et al. 2014; Watkins et al. 2017; Muhlemann et al. 2018). The DPBA signal was most striking at the top of the pistil in stigmatic tissue. The less intense DPBA fluorescence along the stigma also reveals puncta of DPBA on the pistil that are the size and position of nuclei, consistent with prior reports that reveal nuclear accumulation of flavonols in leaf and roots of Arabidopsis and tomato (Saslowsky et al. 2005; Lewis et al. 2011; Watkins et al. 2014, 2017). We also observed that the styles of are appeared thinner than those of VF36, suggesting a role for flavonols in female tissue development.

To determine if reduced levels of flavonols resulted in elevated ROS, we used the $\rm H_2O_2$ selective stain PO1 to ask whether reduced stigma flavonols in *are* relative to VF36 led to elevated levels of ROS in this tissue. PO1 signal is also concentrated in the stigma at substantially higher levels than along the pistil in both genotypes (Fig. 9C), with brighter signal in *are*. The fluorescence levels were quantified by drawing a region of interest around stigmas and quantifying the mean gray values. This analysis revealed 1.4-fold higher PO1 fluorescence in *are* than in VF36 (Fig. 9D). Consistent with the understanding that flavonols provide essential antioxidant capacity to plant tissues, these results demonstrate an inverse relationship between flavonols and ROS on the stigma in both VF36 and *are* (Fig. 9, A and C), which mirrors the difference in pollen tubes, as shown in Fig. 3. We therefore asked how these differences in flavonols and ROS affect pollen tube growth in vivo

Pollen flavonols enhance tube growth through the stigma

To examine the role that the balance between flavonols and ROS plays in the interaction between male and female reproductive tissue, pollen tubes were allowed to grow through pistil explants for 7 h at 28 °C and then visualized with 0.1% decolorized aniline blue (w/v). The are self-cross contained half the number of pollen tubes penetrating through the stigma tissue as VF36, and this reduction was significant (P < 0.05). This defect in pollen tube penetration was reversed by pollinating are pistils with VF36 pollen. However, the reciprocal cross (using are pollen to pollinate VF36 pistils) resulted in similar numbers of pollen tubes as the are self-cross and thus had no rescuing effect (Fig. 9, E and F). Taken together, these findings highlight the importance of flavonols in the tomato pollen grain for a successful pollen–stigma interaction.

Inhibition of respiratory burst oxidase homolog enzymes prevented heat stress-induced ROS and impaired pollen tube elongation

We tested the hypothesis that elevated ROS in response to temperature stress was mediated by NADPH oxidase (NOX)/respiratory burst oxidase homolog (RBOH) enzymes. RBOHs are plasma membrane localized enzymes that produce superoxide in the

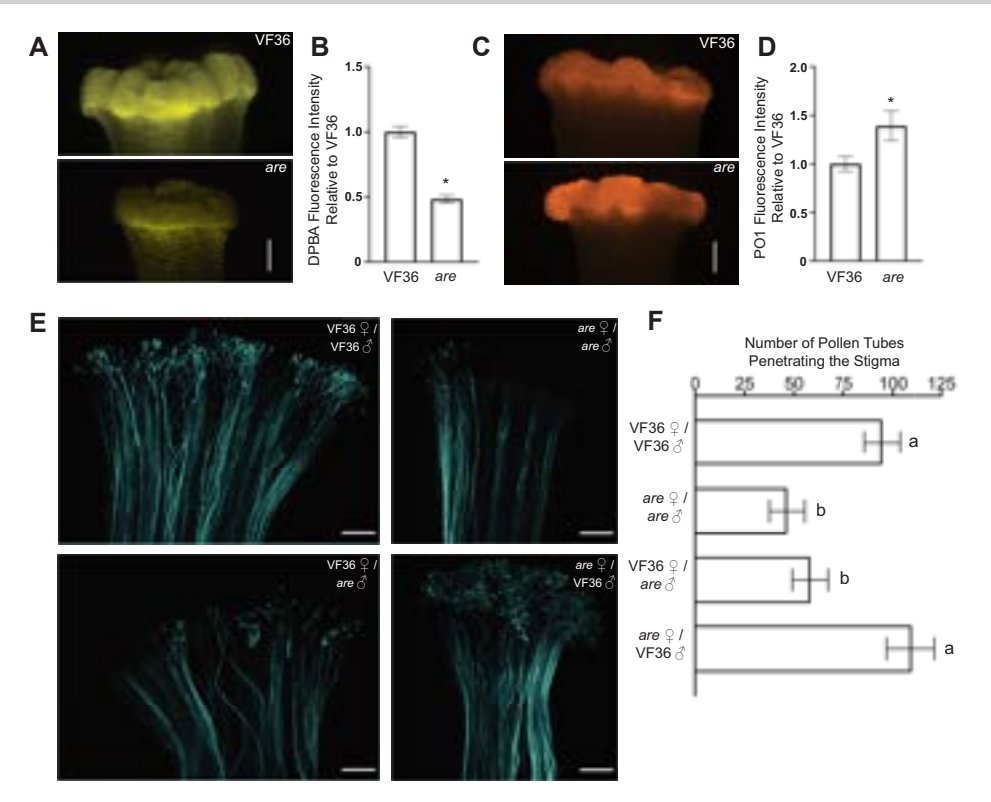


Figure 9. Flavonols in the pollen are necessary for pollen tube penetration through the stigma. A) Representative images of flavonol levels in VF36 and are stigmas as visualized by DPBA staining (yellow). B) The mean and se of DPBA fluorescence intensity in VF36 and are stigmas are reported relative to VF36 levels ($n \ge 9$ stigmas per each genotype from 3 independent experiments). Asterisk denotes a significant difference between VF36 and are according to a Student's t test with P < 0.05. C) Representative images of VF36 and are stigmas stained with PO1 to detect H₂O₂ (orange). D) The mean and se of the mean of PO1 fluorescence intensity are reported relative to the VF36 stigma in VF36 and are stigmas ($n \ge 11$ stigmas per genotype from 4 independent experiments). Asterisk denotes a significant difference between VF36 and are according to a Student's t test with P < 0.05. E) Representative confocal micrographs of pollen tubes growing through the female reproductive tract as visualized by decolorized aniline blue. The contrast and brightness of each image were adjusted differently to maximize visualization of pollen tubes to allow for accurate counting. F) Quantification of the number of pollen tubes that penetrated through the stigma region ± SEM. Different letters denote significant differences according to a 1-way ANOVA followed by a Tukey post hoc test with P < 0.05 ($n \ge 19$ pollinated pistils for each cross from at least 5 independent experiments). The scale bar is 250 μm for all images.

extracellular space. Superoxide can be converted to H_2O_2 by way of SOD and enters cells via aquaporins (Chapman et al. 2019). Consistent with this enzyme being made in pollen, we examined an RNA-seq data set (described below) and identified 2 RBOH genes (SIRBOHE and SIRBOHH) whose transcripts are expressed in tomato pollen, with SIRBOHH being the most highly expressed of the 2 (Supplementary Table S2). Temperature stress did not result in increased expression of either of these RBOHs, but the activity of this class of enzymes is frequently regulated posttranscriptionally (Chapman et al. 2019).

To determine if RBOH enzymes function in increasing ROS in response to elevated temperature we used VAS2870, a highly specific inhibitor of mammalian RBOH activity (Reis et al. 2020) that also inhibits plant RBOH enzymes (Postiglione and Muday 2022), and examined the ability of this inhibitor to reduce ROS and to enhance pollen tube germination and elongation. We germinated pollen grains from VF36 and are flowers in PGM containing $1 \, \mu \text{M}$ VAS2870, or in PGM with a solvent control for 30 min at 28 °C. Pollen was then transferred to 34 °C or kept at 28 °C for an additional 90 min and then labeled with CM-H2DCFDA for 20 min (Fig. 10A). Treatment of VF36 pollen with VAS2870 during the 28 °C incubation did not alter the levels of DCF fluorescence. In contrast, at elevated temperatures, the 2.2-fold increase in DCF fluorescence in VF36 at 34 °C relative to 28 °C was diminished after inhibitor treatment (Fig. 10B). We also observed significant decreases in DCF fluorescence in VAS2870 treated are pollen tubes at both 28 and 34 °C. These results are consistent with the ROS increases at elevated temperature being driven by increased activity (but not synthesis) of RBOH enzymes in pollen.

This reduction in temperature-dependent ROS synthesis in pollen tubes treated with VAS2870 was also reflected by decreased temperature effects on the length of pollen tubes. VF36 and *are* treated with VAS2870 exhibited a 1.3-fold and a 1.5-fold increase, respectively, in pollen tube length at 34 °C as compared to tubes in each genotype without inhibitor (Fig. 10C). However, the disruption of ROS synthesis did not increase pollen tube length in VF36 at 28 °C, but rather led to a 1.5-fold reduction in the length of tubes incubated with VAS2870. This result is consistent with a requirement for RBOH mediated ROS synthesis at the tip of pollen tubes that are required for tip growth as shown using mutants in both Arabidopsis and tomato (Potocký et al. 2007; Kaya et al. 2014; Jiménez-Quesada et al. 2016; Dai et al. 2021). These results indicated that ROS synthesis in this genotype may have been decreased to suboptimal levels for successful tube extension.

We also examined the effects of RBOH inhibition during heat stress on pollen germination rates. Incubation with VAS2870 did not affect VF36 germination at either temperature, but treatment with this inhibitor significantly improved germination of *are* pollen grains by 1.2-fold at 28 °C and 1.6-fold at 34 °C (Fig. 10D). These findings are consistent with RBOH enzymes driving elevated ROS synthesis in response to temperature stress and as the source of damaging ROS that impairs pollen tube growth.

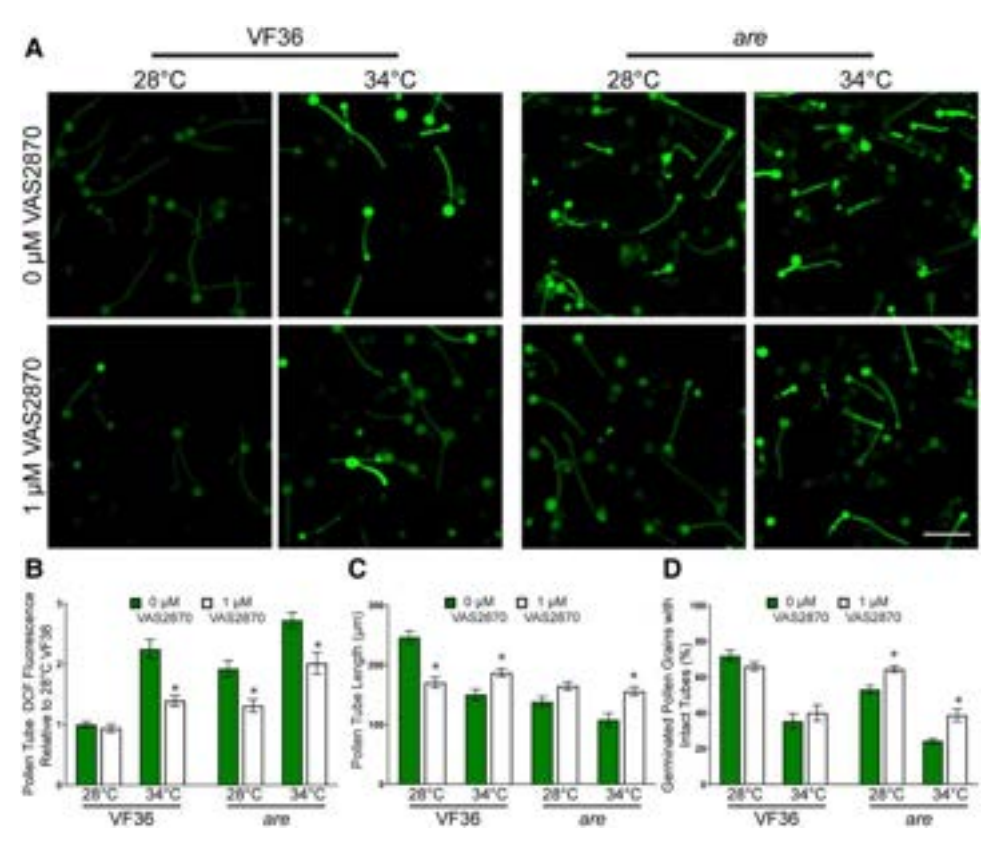


Figure 10. Inhibition of RBOH activity reduces heat-induced ROS accumulation and impaired pollen performance. A) Representative confocal micrographs of DCF fluorescence intensity of elongating pollen tubes treated with 1 μ M of the pan-RBOH inhibitor VAS2870 (green). Quantification of average and SEM of B) DCF fluorescence intensity, C) pollen tube length, and D) germination in PGM containing VAS2870 across 4 independent experiments is reported (n > 200 grains or 62 tubes per genotype and treatment). Pollen was incubated at 28 or 34 °C. Asterisks denote significant differences from 0 μ M VAS2870 treatment within a particular genotype and temperature treatment according to 2-way ANOVA followed by a Tukey post hoc test with a P < 0.05. The scale bar is 100 μ m for all images.

At elevated temperatures, the *are* mutant has more differentially expressed genes than VF36 and VF36-F3H-T3

To provide insight into the mechanisms by which flavonols and elevated temperatures, individually or jointly, control pollen tube germination and elongation, we performed a time course RNA-seq analysis using VF36, are, and VF36-F3H-T3. For each line, mRNA was collected from pollen at 15 and 30 min of germination at either 28 or 34 °C, representing the pollen germination phase. Additionally, we collected mRNA samples from pollen tubes that were germinated at 28 °C for 30 min and then either kept at that temperature or transferred to 34 °C for an additional 45 or 75 min (75 or 105 min of total growth), representing the pollen tube elongation phase (Supplementary Fig. S5). These timepoints are when are had impaired pollen germination and pollen tube growth and elevated ROS levels as indicated by light microscopy of pollen morphology and DCF fluorescence, respectively.

RNA was then isolated for each sample, and samples were utilized for paired-end, strand-specific RNA sequencing. We uploaded the reads of all samples into Integrated Genome Browser (Freese et al. 2016) and examined the F3H gene (PRAM_26184.1 in tomato genome version SL5, formerly solyc02g083860 in genome version SL4). We verified the presence of the are point mutation, which is in the 47,450,716 position in the F3H gene in which a C is replaced with a T (Supplementary Fig. S6). This mutation is absent in all other samples.

We conducted a principal component analysis (PCA) using the top 500 most variable genes to investigate similarities in the transcriptome-wide expression profiles (Fig. 11A). Principal component 1 (PC1) explains 58% of the variance in expression profiles and clearly separates the *are* samples from VF36 and VF36-T3 samples. PC2 explains 18% of the variance and clearly separates samples by time and temperature stress, with later timepoints and higher temperature stress in all 3 genotypes distinct from earlier and nonheat-stressed samples. Analysis of *are* samples separately shows a strong PC1 (69% explained) that again corresponds with time and temperature (Fig. 11B). Similarly, analyses of VF36 and VF36-T3 by themselves separate on PC1 by time and PC2 by elevated temperature (Fig. 11, C and D). This difference is accentuated in the timepoints taken during the pollen tube elongation phase, which were exposed to the 34 °C temperature for 45 or 75 min.

Differentially expressed genes (DEGs) significant at adjusted P < 0.05 and log₂ fold change (log₂FC) of greater than or less than 1 between 28 and 34 °C increased over the time course, with at least twice as many DEGs detected in *are* than VF36 or VF36-T3 at every timepoint (Fig. 12A, Supplementary Data Sets 1 to 3). Differential gene expression analysis of the 75-min pollen tube samples at 34 to 28 °C for *are*, VF36, and VF36-T3 detected only DEGs that were upregulated at the higher temperature in all 3 genotypes (Fig. 12, B to D). This pattern of a strong majority of significant DEGs being upregulated is similarly found at all timepoints (Supplementary Figs. S7 to S9).

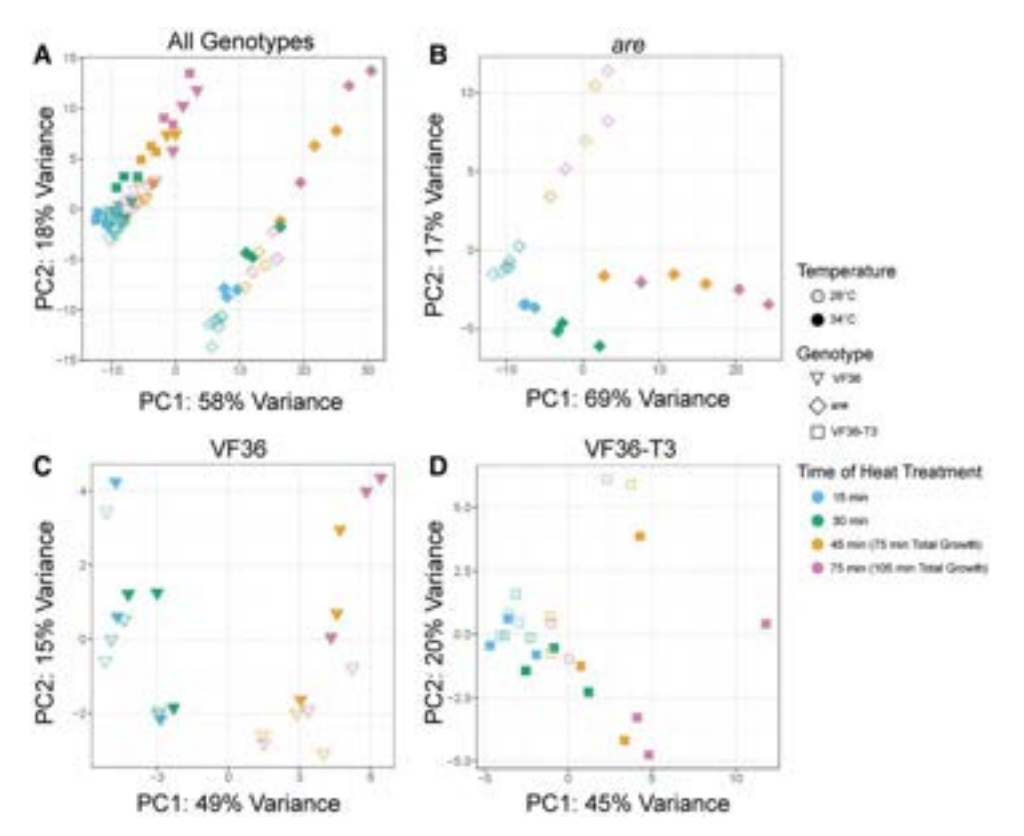


Figure 11. PCA plots highlight distinct transcriptional responses between are and the other 2 genotypes and in response to elevated temperature. A) PCA plot for all samples analyzed via RNA-seq. The samples in the right cluster are all are samples, while the group on the left contains both VF36 and the VF36-T3 samples. Individual PCA plots for each genotype reveal the time and temperature response within each genotype with B) are, C) VF36, and D) VF36-T3 samples.

We generated volcano plots of VF36, are, and VF36-F3H-T3 at all 4 timepoints. The differentially expressed (DE) genes within genotype in 34 °C samples relative to 28 °C samples are shown at the 75-min timepoint (105 min total growth) (Fig. 12, B to D). These volcano plots demonstrate that the majority of the heatdependent DE genes are upregulated and there are greater numbers of DE genes in are compared to the other 2 genotypes. The volcano plots for all the other timepoints are available as Supplementary Figs. S7 to S9. These additional plots illustrate that the majority of temperature-dependent DE genes are increased at the higher temperature across all timepoints.

The number and rate of transcript abundance changes are greater in *are* than other genotypes

To further compare how the heat-dependent transcriptional responses differed between are, VF36, and VF36-T3, we determined how many DE genes were shared between these genotypes. For this comparison, we evaluated the significant DEGs based on temperature at the 75 min timepoint (105 min total growth), as this timepoint contained the largest number of DEGs. The UpSet plot in Fig. 13A shows that the largest group of DEGs are 74 are-specific DEGs, followed by 41 DEGs shared among all 3 genotypes, after which the DEG overlaps are trivially smaller (Fig. 13A). This result illustrates that a strong majority of VF36 and VF36-T3 DEGs were also DE in are, but that are also had a substantial number of additional DEGs not found in VF36 or VF36-T3.

We examined the functional annotation of the DEGs in the 75 min are samples when the transcript abundance was compared between the 28 and 34 °C samples and found that these DEGs were enriched in Gene Ontology (GO) annotation for "response to stress," "response to heat," and other GO categories relating to H₂O₂, as expected given the experimental treatment and our biochemical results that showed the treatment elevated ROS. The other enriched GO terms include "protein folding," "protein complex formation," and "chaperone dependent protein folding," which reflect the expected synthesis of proteins that functions to reduce the effects of heat that denatures proteins. The notable number of are-specific temperature-responsive DEGs is accompanied by several are-specific functional enrichments, such as "protein-containing complex assembly," "protein complex oligomerization," "chaperone cofactor-dependent refolding," and "response to hydrogen peroxide" (Fig. 13B). The are-specific DEGs also include a variety of antioxidant enzymes belonging to the glutathione S-transferase, ascorbate peroxidase, and thioredoxin families, an intriguing finding that suggests alternative mechanisms of ROS homeostasis are activated in are pollen to compensate for the lack of flavonol antioxidants (Fig. 13B).

To determine if there were genotype-specific differences in the heat stress response of temperature-responsive DEGs, we calculated the log₂FC at 34 °C relative to the 28 °C sample for each timepoint and then evaluated transcripts that were DE in at least 2 genotypes at the 75 min timepoint (105 min total growth) (Supplementary Figs. S10 to S12). Using these 56 transcripts that were DE in at least 2 genotypes, we sought to identify groups of transcripts with highly similar temporal responses to each other in VF36 and are, as these groups might represent temperature-responsive functional subnetworks. To achieve this analysis, we employed the Partitioned Local Depths (PaLD) approach (Berenhaut et al. 2022; Khoury et al. 2023), which uses

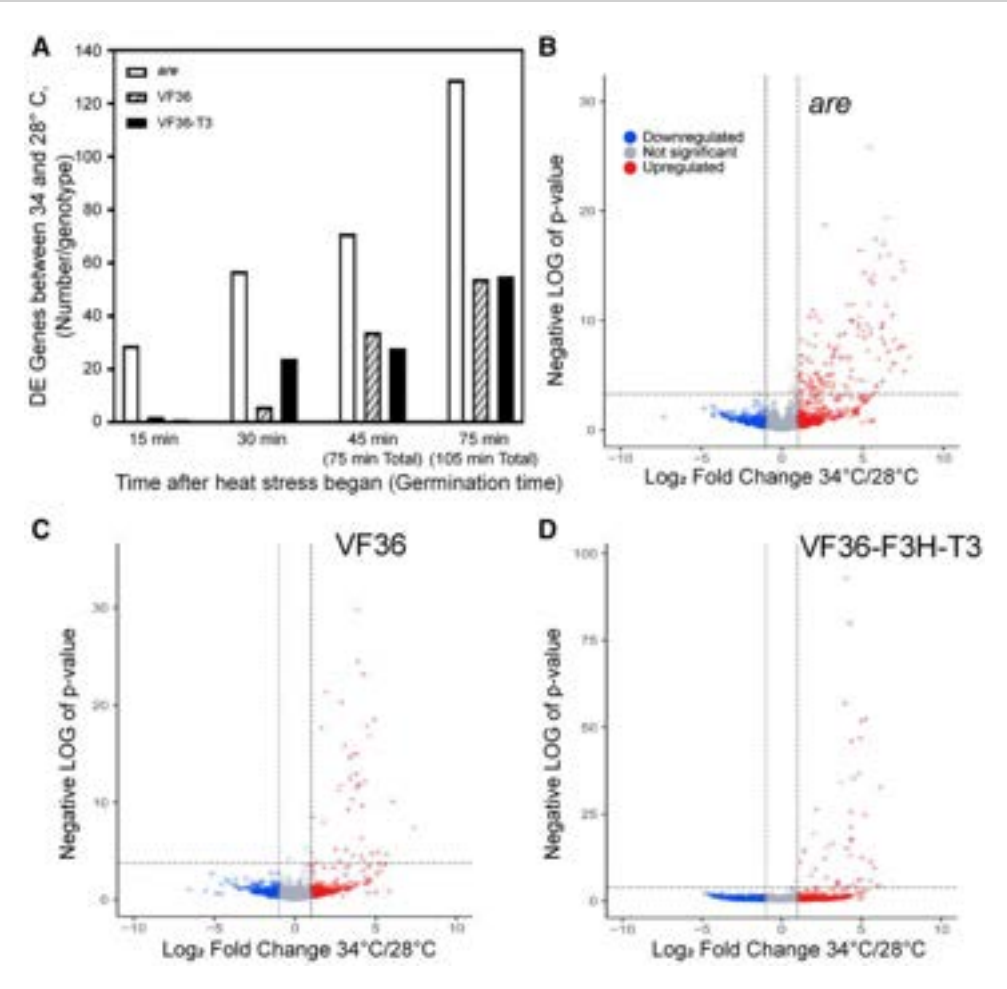


Figure 12. Transcriptional responses increase across the duration of temperature stress and are accentuated in the *are* mutant. A) The number of DE genes at 34 °C relative to 28 °C within each genotype as determined using EdgeR is graphed as a function of time of pollen tube growth for VF36, *are*, and VF36-F3H-T3. These genes were defined as DE if they had an adjusted P < 0.05 and log fold change greater than or less than 1. B to D) Volcano plots of the log fold change at 34 °C relative to 28 °C and P-values for all samples. The dotted lines represent P-value cutoffs of 0.05 and log₂FC of 1. B) *are*, C) VF36, and D) VF36-F3H-T3. Blue circles denote genes that are downregulated (log₂FC below 1), red crosses indicate genes that are upregulated (log₂FC above 1), while gray circles denote genes that do not display a log₂FC above or below the cutoff of 1.

values of cohesion to generate a network of the relationships among a set of genes including local (i.e. direct connections between transcripts) and global relationships (i.e. indirect connections among larger communities of transcripts).

PaLD analysis of the 56 DEGs revealed a network consisting of 2 communities whose members had similar responses to each other in VF36 and are and 7 isolated transcripts that had unique responses in these genotypes (Fig. 13C). Among the largest group, Group 1, we observed 3 smaller subnetworks which we denoted as 1A, 1B, and 1C on the network (Fig. 13C) and heatmap (Fig. 13D, Supplementary Data Set 4). These subgroups were defined by transcripts that had relatively slower upregulation in VF36 and faster upregulation in are and mostly consisted of transcripts that encoded heat shock proteins (Fig. 13D). On the other hand, the second largest group, Group 2, was defined by transcripts that responded relatively quickly in both VF36 and are (Fig. 13D). Unlike Group 1, Group 2 had several transcripts that encoded proteins involved in metabolism, representing heat-responsive metabolic genes that are independent of the abundance of flavonols. The 56 DEGs are upregulated more rapidly and to a higher magnitude in are than in VF36 and VF36-T3 (Fig. 13D). Notably, most DEGs are regulated similarly in VF36 and VF36-T3 with few unique genes in either genotype

(Fig. 13D), suggesting the improved pollen performance seen in VF36-T3 is not based on a differential regulation in response to heat. On the other hand, *are* contains many unique genes that were not found to be differentially regulated in the other 2 genotypes (Fig. 13A). This group of genes may yield important candidates for future targets to prevent the damaging effects of elevated temperatures.

We also examined the transcriptional regulation of the F3H gene in *are* and VF36 pollen. Intriguingly, F3H expression was elevated in *are* when compared to VF36 and VF36-F3H-T3 at all timepoints and temperatures (Supplementary Table S2). This is consistent with the point mutation in *are* producing a full transcript, and with the absence of a flavonol intermediate that acts as a negative feedback signal to decrease F3H transcription. Together, these data indicate that heat-driven transcriptional responses in tomato pollen differ with levels of flavonols, as well as the length of exposure to increased temperature.

Pollen from *are* exhibits a differential transcriptional baseline than VF36

Our finding of increased transcriptional response of *are* to heat stress provides greater insight into the poor performance of pollen

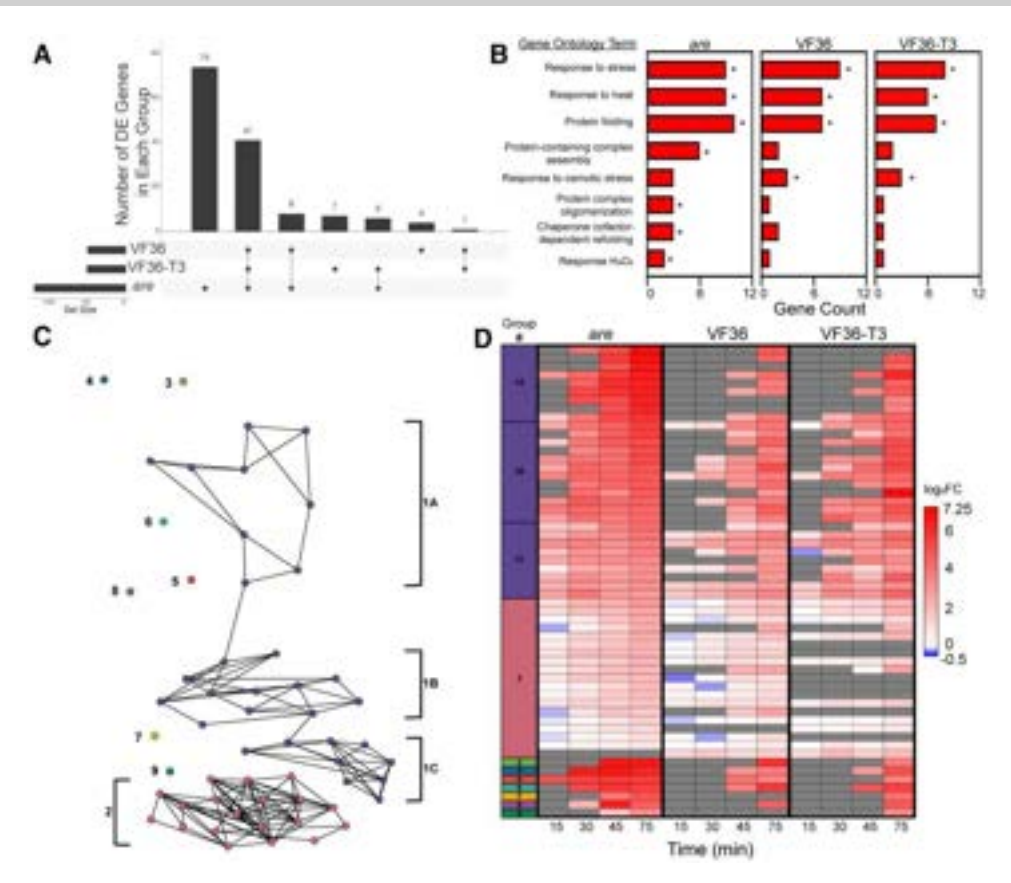


Figure 13. The heat-dependent transcriptional response of are occurs more rapidly and contains a greater number of unique transcripts. A) Upset plot of temperature-dependent DE genes within each genotype after 75 min heat treatment (105 min total growth). Numbers above bars represent the number of temperature-regulated DE genes that are shared between genotypes connected by lines. Set size refers to the number of DE genes at this specific timepoint for each genotype. B) Biological processes that are significantly enriched in transcripts that are DE at the elevated temperature in the are mutant were determined using String. Groups that were significantly enriched in the are mutant are reported. The number of genes in each group was determined for the other genotypes. Asterisk indicates the groups for which enrichment was significant relative to genome. C) PaLD generated network of 56 genes that were found to be DE in 2 or more genotypes after 75 min heat treatment (105 min total growth) with nodes color coded for each group of like responding transcripts. D) Heatmap of the 56 genes used in the PaLD analysis, with the first column representing the PaLD groups from C) (Khoury et al. 2023). The temperature-dependent log₂FC of these genes was then mapped back to pollen samples taken at the earlier timepoints. Gray boxes represent no detected expression at that timepoint.

from this genotype at elevated temperatures. However, this analysis does not explain the impaired pollen performance observed in are at optimal temperatures. To understand how are differs from its parental line at each timepoint and temperature, another DE analysis was performed comparing VF36 to are at each developmental timepoint and temperature (Supplementary Data Set 5). This comparison revealed consistent differences in transcript abundance between these genotypes at all pollen developmental stages across this time course. Across the time course, we found 20 are-specific DEGs in common among all timepoints, with a maximum of 79 at 34 °C at 2 timepoints (Supplementary Table S3). As shown here in other analyses, genotype-dependent DEGs increased with elevated temperature, particularly at the later stages of the time course. The relative abundance of transcripts in are relative to VF36 was calculated for the 20 DEGs that had significant differences at all 4 timepoints, with a majority of these genes having higher abundance in are (Supplementary Fig. S13).

We also examined a core set of genes encoding 36 heat shock proteins, heat shock transcription factors, or molecular chaperones that were temperature-dependent DEGs within each genotype (shown in Fig. 13C). We calculated the log₂FC for these genes when the transcript abundance at 28 °C in are was reported relative to VF36 in time and temperature matched samples

(Fig. 14, Supplementary Data Set 5). Of these 36 genes, 29 were upregulated in are pollen at optimal temperatures at all developmental stages beginning with the 15-min timepoint. This analysis suggests that, even at a near-optimal 28 °C, are contains a different transcriptional setpoint than VF36 and are pollen transcriptionally reflects the stress of elevated ROS and the resulting protein unfolding.

Discussion

Exposure of plants to temperatures above the optimal range can have a deleterious effect on multiple stages of reproductive and vegetative growth and development, resulting in critical reductions in crop yield at elevated temperatures (Sato et al. 2006; Fahad et al. 2017; Rieu et al. 2017; Begcy et al. 2019; Chaturvedi et al. 2021). An increase of as little as 4 to 6 °C above optimal temperatures during pollen germination and tube elongation both increases ROS and reduces pollen performance (Muhlemann et al. 2018; Wu et al. 2020). While localized, temporally coordinated ROS bursts are required at each stage of pollen growth and development (Potocký et al. 2007; Johnson et al. 2019; Daryanavard et al. 2023; Ali and Muday 2023), ROS overaccumulation at inappropriate development stages can reduce crop yield (Mittler

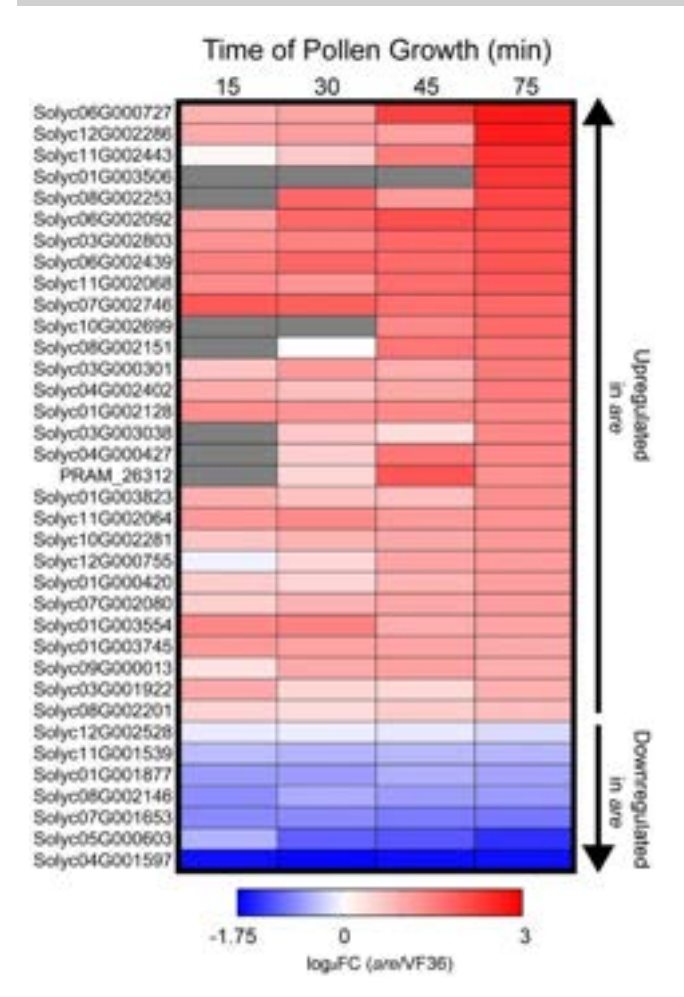


Figure 14. The *are* mutant displays an upregulated heat response even at optimal temperatures. Heatmap of the 36 genes encoding heat shock factors that were found between *are* and VF36 at 28 °C. log₂FC of *are* relative to VF36 for these genes was then mapped back to pollen samples taken at the earlier timepoints. Genes are ranked by highest logFC in *are* at the 75 min timepoint (105 min total growth). Gray boxes represent no detected expression at that timepoint.

2002; Speranza et al. 2012; Muhlemann et al. 2018; Gong et al. 2024). Plants synthesize antioxidant proteins and specialized metabolites, including flavonols, as a protective measure against these damaging ROS changes, and mutants that make no flavonols have impaired or failed reproduction (Schijlen et al. 2007; Muhlemann et al. 2018; Wang et al. 2020; Daryanavard et al. 2023).

Muhlemann et al. (2018) reported that under optimal temperature conditions, the impaired pollen performance of are was reversed by complementation with a wild-type copy of the F3H gene, showing that pollen germination, tube elongation, and tube integrity, as well as ROS levels, were restored to wild-type levels (Muhlemann et al. 2018). In this article, we evaluated the hypersensitivity of are to elevated temperature and asked whether flavonols protect a broad range of pollen processes, including pollen development, germination, and tube extension, from the negative effects of heat stress by examination of a complemented mutant line and plants engineered to overproduce flavonols or treated with exogenous flavonols. We examined temperature effects on ROS levels in each of the genotypes and treatments to determine if the protection conveyed by flavonols is to maintain ROS homeostasis. Finally, we asked whether heat-dependent changes in the pollen transcriptome were

amplified in *are*, consistent with elevated ROS driving transcriptome remodeling.

The tomato mutant are contains a point mutation in the gene encoding the F3H enzyme resulting in reduced synthesis of flavonoids, which include flavonols and the downstream metabolites, anthocyanins (Maloney et al. 2014). The are mutant has alterations in root development including reduced lateral root formation and increased root hair formation (Maloney et al. 2014) as well as altered guard cell closure in response to ABA treatment (Watkins et al. 2017). Aspects of each of these are phenotypes can be attributed to higher levels of ROS relative to VF36, its parental line. The performance of are pollen is impaired under optimal growth conditions, resulting in a significant reduction in seed set when compared to VF36 (Muhlemann et al. 2018). Previous studies in rice, tomato, and petunia have also found that mutations that disrupt flavonol biosynthesis impaired pollen development and function, as well as reduced fruit yield and seed set (Mo et al. 1992; Schijlen et al. 2007; Wang et al. 2020). A recent paper also found that the Arabidopsis transparent testa (tt4) mutant, with a mutation in the single gene encoding the first enzyme of flavonoid synthesis, chalcone synthase, which produces no flavonols, also has impaired performance at elevated temperature (Xue et al. 2023). In this study, we focus on the molecular mechanisms by which heat stress leads to impaired pollen performance, the effects that flavonols play in the alteration of these mechanisms, and whether increased flavonol synthesis can be used as a strategy to enhance pollen growth and development during exposure to elevated temperatures.

We evaluated the effects of flavonols on pollen yield, pollen viability, and pollen tube elongation when exposed to temperature stress, using the are mutant, its wild-type parental line, VF36, and each genotype transformed with a Pro35S:F3H gene. Previously, are was transformed with an F3H gene driven by the constitutive CaMV-35S promoter, with the line are-F3H-T5 (are-T5) being the best characterized transformation, as well as the VF36-F3H-T3 (VF36-T3) line transformed with this same construct to overproduce flavonols (Maloney et al. 2014). We utilized these same lines and demonstrated that genetic complementation rescued the impaired pollen performance in are, especially at elevated temperatures. The significant reduction in the pollen yield in are was reversed in the are-F3H-T5 transgenic lines, while the VF36-F3H-T3 line had greater yield. The number of viable pollen grains and the elongation of pollen tubes at optimal and elevated temperatures were also evaluated in these 4 genotypes, revealing negative effects in VF36 that were accentuated in are, were reversed in are-F3H-T5, and were abolished in the VF36-F3H-T3 line. Of greatest note, transformation with an F3H gene in VF36 resulted in protection of pollen from temperature stress in these same assays, resulting in substantially higher viability, germination, tube growth, and pollen tube integrity than in VF36. This result suggests that engineering or breeding plants to have elevated flavonols in pollen may protect plants from temperature stress.

We also examined whether the impaired pollen germination in are was directly tied to reduced levels of flavonols in these genotypes, rather than elevated levels of naringenin, a flavonol precursor and the metabolite directly before the F3H enzyme. We compared rates of pollen germination at optimal and elevated temperatures in are and VF36 in the absence and presence of exogenous application of flavonols. We incubated both are and VF36 with the 3 most prevalent flavonols in tomato: kaempferol, quercetin, or myricetin. As little as 5 μ M of each flavonol was able to reverse the impaired germination in are, with the most profound effects evident in the presence of temperature stress. These

findings are consistent with a previous report utilizing a petunia chs mutant that showed that chemical complementation with these 3 same flavonols at optimal temperatures partially rescued pollen germination (Mo et al. 1992), with kaempferol being the most potent at restoring germination with chemical supplementation (Pollak et al. 1993). This study shows that chemical application of flavonols to pollen can confer heat tolerance and reverse the temperature hypersensitivity in a mutant with impaired endogenous flavonol synthesis.

The role of flavonols in protecting pollen from heat stress through their action as antioxidants (Daryanavard et al. 2023) was tested by examining ROS levels in are, VF36 and the are-F3H-T5 line using the general ROS indicator CM H₂DCFDA, which is oxidized by multiple forms of ROS to become the fluorescent product DCF, and with PO1, which is selective for H2O2. At both elevated and optimal temperatures, are pollen showed elevated DCF fluorescence in both pollen grains and tubes relative to VF36 pollen. Both genotypes had elevated ROS at 34 °C compared to their 28 °C controls, with are pollen at 34 °C having the highest overall DCF fluorescence intensity. The accumulation of ROS in germinating pollen grains and elongating tubes in are-T5 was reduced at both 28 and 34 °C relative to are at those same temperatures and relative to VF36 at 34 °C. Additionally treatment with kaempferol had a similar effect on ROS levels and pollen germination. Measurement of PO1 fluorescence in pollen tubes of these 4 genotypes followed similar trends, with statistically significant increases in PO1 fluorescence in are and VF36 at 34 °C compared to 28 $^{\circ}\text{C}$ with higher levels at the pollen tube tip. In both genotypes, the presence of the Pro35S:F3H construct prevented temperature-induced PO1 signal increases. These results demonstrate that both genetic and chemical complementation reversed the effect of the are mutation on ROS accumulation and pollen performance and even raised germination under heat stress to levels that were higher than in the VF36 parental line. These observations suggest that the impairments in VF36 at elevated temperatures and the reductions in pollen germination and tube elongation in are at both temperatures were due to the overaccumulation of ROS.

The ability of the VF36-F3H-T3 line to be insensitive to the effects of high temperature on pollen viability, germination, and tube growth and to maintain constant levels of ROS at elevated temperatures during the pollen germination and pollen tube elongation phases are exciting results. These findings provide evidence for the mechanism by which the F3H overexpression enhances thermotolerance when exposed to high-temperature stress. Collectively, these data suggest that increasing flavonol biosynthesis reduced levels of ROS to protect pollen from oxidative damage, which may have applications in breeding or engineering crops to protect pollen from temperature-induced ROS and the resulting impairments to pollen performance.

We sought to understand the role of flavonols during the pollen-stigma interaction to determine if reduced levels of flavonols in maternal tissues impacted pollen tube growth in vivo and whether wild-type levels of stigma and pistil flavonols could reverse the reduction of are pollen tube growth. We demonstrated that in the are stigma there are reduced levels of flavonols and elevated levels of ROS as compared to the parental line, as quantified by DPBA and PO1 fluorescence, respectively. The number of pollen tubes that were able to penetrate through the stigma was reduced in an are self-cross compared to VF36 self-cross. A prior publication using a parthenocarpic tomato CHS-RNAi line with reduced flavonol levels showed that crosses of this line with a wild-type line, as either the pollen donor or the pistil, led to improved fertility relative to the CHS-RNAi line (Schijlen et al. 2007). Their images of pollen tubes growing through the pistil were also consistent with improved performance of pollen or pistils from the CHS-RNAi line when crossed with wild-type. We therefore hypothesized that VF36 pollen and pistils would reduce the effect of the are mutation on pollen tube growth.

We quantified the number of pollen tubes that were able to transverse the stigma and found that the are mutation only reduced the numbers of pollen tubes when are was the pollen donor and that are pollen tube growth was not improved when tubes grew through a VF36 stigma. The finding that female tissue was unable to biochemically complement flavonol-reduced pollen growing through the stigma is consistent with in vivo pollen growth assays in rice (Wang et al. 2020) but not with the CHS-RNAi tomato results (Schijlen et al. 2007). Our analysis did not include quantification of the tubes that reached the base of the pistil and the ovaries, so it is possible that the role of pistil flavonols is stronger as the pollen tubes elongate greater distances. Additional detailed analyses of are pollen growth in vivo through pistils with a range of flavonol levels is necessary to fully address this question. Another explanation for these different results is that the flavonol deficiency in are pistils is less extreme than in the CHS-RNAi tomato lines. Leaf and fruit peel extracts of the CHS-RNAi tomato lines had 10% of the flavonoids as the wild-type and formed parthenocarpic fruits. In contrast, are pollen tubes contain half the flavonols as wild-type as measured by DPBA staining and are fruits are able to form reduced numbers of seeds under optimal temperature conditions relative to the parental line (Muhlemann et al. 2018). This more subtle difference might make it harder to detect the role of pistil flavonols.

We also evaluated whether the inhibition of enzymatic drivers of ROS synthesis would be able to block temperature stress-induced ROS. ROS can be produced by many sources, including electron transport in metabolic organelles and enzymes such as RBOHs/NOX (Møller et al. 2007; Martin et al. 2022; Postiglione and Muday 2022). We detected transcripts encoding 2 RBOH enzymes that are expressed in tomato pollen. Therefore, we asked whether temperature-induced ROS acted via RBOH enzymes by incubating pollen with the selective, pan-RBOH inhibitor, VAS2870, which targets an active-site cysteine that is conserved across mammalian NOX enzymes as well as RBOHs in plants (Yun et al. 2011), providing increased specificity over other inhibitors such as DPI (Mangano et al. 2017; Postiglione and Muday 2022).

RBOH inhibition blunted the increased ROS accumulation after incubation at 34 °C in pollen tubes in our 4 core genotypes. This inhibitor reduced the negative effect of high temperature on pollen tube length when compared to pollen at elevated temperature that did not receive the inhibitor. These findings are in agreement with other studies that indicate that RBOH-produced ROS at the tube tip is required for pollen tube growth (Potocký et al. 2007; Speranza et al. 2012; Kaya et al. 2014; Jiménez-Quesada et al. 2016; Muhlemann et al. 2018; Jimenez-Quesada et al. 2019), as evidenced by the reduced pollen tube length in VF36 at optimal temperatures after treatment with VAS2870. However, we also show that RBOHs contribute to heat-dependent ROS overaccumulation, and RBOH inhibitor treatment can protect are from ROS increases during heat stress and improve performance of this genotype at both optimal and elevated temperatures.

To better understand the molecular mechanisms by which temperature affected the function of germinating pollen grains and elongating pollen tubes, we examined the transcriptome in VF36, are, and the VF36-F3H-T3 transgenic line at optimal and elevated temperatures at 4 timepoints during pollen germination (15 or 30 min after hydration) and pollen tube elongation (75 and 105 min after hydration) reflecting the peak rate of pollen tube elongation. We identified DE transcripts at 34 °C as compared to 28 °C in all genotypes, revealing that the number of DE genes was substantially higher in are. There were increasing numbers of DE transcripts in pollen grains and tubes as the duration of the heat stress period increased. There was a large group of DE genes that were shared between all genotypes with almost all of them increasing with elevated temperature, with heat maps revealing the greater rate and magnitude of these responses in are. Among these shared DE genes are multiple heat shock proteins, chaperones, and heat shock transcription factors, which have significantly enriched annotations as revealed by a GO annotation analysis. These groups of DE genes are consistent with the previously reported transcriptional response to heat stress in tomato pollen (Frank et al. 2009). The differential remodeling of the transcriptome of male reproductive tissues after exposure to elevated temperatures between tomato lines with different levels of thermosensitivity is in agreement with a prior report evaluating the transcriptome of meiotic anthers (Bita et al. 2011).

We did identify a large number of DE transcripts that were increased in are in response to heat stress, but not in VF36 or VF36-F3H-T3, which is most evident in the UpSet plot in Fig. 13A. We also found that the DE genes in are also had enriched annotations not found in the other genotypes including chaperone cofactor-dependent refolding and response to H₂O₂, suggesting an enhanced temperature stress effect in are pollen. These responses may be linked to the elevated ROS in are, which through oxidation of cysteine residues to form cysteine sulfenic acids can reversibly oxidize proteins to alter their structure (Garrido Ruiz et al. 2022) compounding the effect of elevated temperature on protein denaturation. We also used a community detection algorithm, PaLD, to build a network revealing the groups of genes with the most common transcriptional response to elevated temperature across the are and VF36 genotypes, when we consider the changes in transcript abundance in response to temperature (Khoury et al. 2023).

To explore whether there are differential transcriptional responses in *are* in the absence of temperature stress, we performed a DE analysis between *are* and VF36 at all timepoints and temperatures. This analysis revealed a group of genes that were DE at all timepoints and temperatures, with increasing number of DE genes between genotypes at 34 °C, consistent with the greater temperature-dependent increases in DE genes in *are* when comparisons were made within genotypes. When comparing the transcriptional baselines of *are* to VF36 at optimal temperatures, we identified a group of 36 genes that are involved in the heat stress response and are upregulated in *are* as early as the 15-min timepoint. This finding suggests that *are* pollen may have altered protein folding due to elevated ROS even at optimal temperatures leading to impaired pollen performance in *are* even at 28 °C.

These results reveal that an increase of flavonol levels above wild-type levels can act as an avenue to protect tomato pollen from the deleterious effects of elevated temperature stress. Consistent with this finding, a 2-fold increase in flavonols in tomato pollen after growth at 38 °C has been reported (Paupière et al. 2017), and pollen of 2 tomato cultivars 'Saladette' and 'CLN1621' had increased pollen viability under heat stress and had 2-fold higher levels of flavonols than thermosensitive 'Money Maker' and 'M82' (Dinar and Rudich 1985; Firon et al. 2006; Xu et al. 2017), suggesting that plants may produce flavonols to protect against temperature-induced ROS.

We showed that diminished flavonol synthesis in a tomato mutant, such as are, critically reduces tolerance to elevated temperatures in pollen reducing both pollen performance tied to elevated levels of ROS consistent with the diminished levels of flavonol antioxidants. These temperature-dependent effects can be rescued with both exogenous flavonol treatment as well as engineering plants with the F3H transgene to increase flavonol biosynthesis and protect pollen from heat stress. We also demonstrated a role for RBOH enzymes in temperature-dependent ROS synthesis. Additionally, our data reveal a robust transcriptional response to elevated temperatures that is accentuated by reduced levels of flavonols in pollen grains and tubes and may provide additional candidate genes to improve thermotolerance in crop plants. Flavonols are critical for plants to adequately respond to and recover from the detrimental effects of heat stress in male reproductive tissue. Our findings provide an intriguing potential avenue to engineer crop plants with elevated flavonols to improve tolerance to elevated temperatures.

Materials and methods Plant material and growth conditions

Seeds of wild-type (VF36) tomato (S. lycopersicum) and the are mutant were obtained from the Tomato Genetic Resource Center (https://tgrc.ucdavis.edu), and Pro35S:F3H transgenic lines in the are and VF36 backgrounds including are-F3H-T5, are-F3H-T6, VF36-F3H-T3, and VF36-F3H-T5 (abbreviated are-T5, are-T6, VF36-T3, or VF36-T5) were from Maloney et al. (2014), where they were referred to as VF36 or are OE lines. The seeds of VF36 transformed with a ProLAT52:GFP line were from Sheilla McCormack (Zhang et al. 2008); this transgene was crossed into are, and the homozygosity of transgenes and the mutations was verified using PCR and the loss of an Sml1 restriction site in are due to the G to A mutation within the F3H gene.

Tomato seeds were germinated in Sunshine MVP RSi soil and grown under 16 h day (150 $\mu \rm mol/m^2/s$ cool white fluorescent light and 8 h nights at room temperature for 3 to 4 wk). Plants were then transferred to the Wake Forest University greenhouse where they were grown in the same growth media to which lime and Miracle-Gro Shake 'N Feed fertilizer were added. Plants were grown under daylight conditions with no supplemental light, where they began to flower after 6 wk of additional growth. Pollen was also obtained from plants that were propagated by cuttings. Unless noted otherwise, all pollen was harvested from greenhouse grown plants with day temperatures set to 28 °C and night temperature to 21 °C. Pollen was recovered from flowers using less than 20 s of vibration with a custom modified electric toothbrush with a metal bracket that surrounds the anther, collecting pollen into a microcentrifuge tube.

Quantification of pollen yield

Pollen from 3 flowers for each line was harvested as described above and placed in individual 0.7-mL microcentrifuge tubes for evaluation of pollen yield. Released pollen was resuspended in 60 μ L PVS (290 mm sucrose, 1.27 mm Ca(NO₃)₂, 0.16 mm boric acid, 1 mm KNO₃), and then equal volume of 0.4% trypan blue (w/v) staining solution was added to each tube. Pollen grains were quantified by pipetting 10 μ L pollen suspension into Countess Cell Counting Chamber Slides to be counted by a Countess II Automated Cell Counter (Invitrogen). Settings were adjusted to select only mature, viable grains that are, on average, 1.5-fold larger in diameter than nonviable grains, display 2-fold

increased roundness, and have the ability to form a tube. Grains judged as dead are smaller, oblong, much darker, and do not have the ability to form a pollen tube and were gated out of the quantification (Supplementary Fig. S14). Four technical replicates were taken from each tube and averaged, and then pollen concentrations were calculated to reflect the total volume of solution in each tube to give the number of live pollen grains per flower.

Pollen viability assay

Pollen from 3 flowers at anthesis from each genotype was harvested by agitation with an electric toothbrush modified for efficient pollen harvesting into a 0.7-µL microcentrifuge tube. Pollen was then resuspended in PVS (290 mm sucrose, 1.27 mm Ca(NO₃)₂, 0.16 mm boric acid, 1 mm KNO₃), which included 0.001% FDA (w/v) and 10 µm PI. Pollen grains were stained for 15 min at 28 °C and then centrifuged. PVS containing FDA and PI was replaced with PVS alone. The stained pollen was placed on a microscope slide and imaged by confocal microscopy on a Zeiss 880 LSCM microscope using a 10x/0.5 NA Plan-Apochromat objective. FDA was excited with a 488-nm laser, and intensity was collected with an emission window of 490 to 552 nm with maximum laser power of 0.7% and detector gain of 780. PI was excited with a 561-nm laser line while its fluorescent signal was collected within a 584 to 718 nm emission window with maximum laser power of 0.07% and detector gain of 780. Quantifications of viable and dead pollen grains was performed using Fiji in which pollen grains with FDA emission peaking at 500 nm were counted as viable and pollen with PI emission within the grain above 600 were counted as dead grains.

Pollen germination and pollen tube elongation

Flowers were collected at anthesis from greenhouse grown plants, and, in most experiments, pollen was harvested as described above. In rare cases, anthers were detached, and the tips of the anthers were then cut and placed into a microfuge tube and pollen was released by agitation with a vortex. Pollen was then resuspended in 300 µL of PGM (24% [w/v] PEG4000, 0.01 [w/v] boric acid, 2% [w/v] sucrose, 2 mм HEPES pH 6.0, 3 mм Ca(NO₃)₂, 0.02% [w/v] MgSO₄, 0.01% [w/v] KNO₃), which was preequilibrated to either 28 or 34 °C. The entire volume of resuspended pollen was transferred into a sterile 24-well plate and imaged using an Olympus IX2-UCB inverted microscope with a 10x objective and a Tucsen Dhyana CMOS camera fitted with a Tokai HIT-heated

For pollen germination analysis, pollen was incubated at either 28 or 34 °C for 30 min, and images were collected every 2 min using this Olympus microscope. Percent germination was then quantified using Fiji (ImageJ) in which the number of germinated grains was reported relative to viable mature grains based on the criteria described previously. Supplementary Fig. S14 displays a bright field image displaying morphological differences between mature, viable pollen grains and nonviable dead grains. For pollen tube elongation, pollen was incubated at 28 °C for 30 min, heattreated samples were then moved to an incubator at 34 °C for 90 min while control samples remained at 28 °C for an additional 90 min. Pollen tube length was measured from the tip of the pollen tube to the point of emergence on the grain.

PO1 staining of pollen tubes and pistils

For PO1 imaging of samples with elongated pollen tubes, harvested pollen was incubated in PGM at 28 °C for 30 min. Heat-treated samples were then transferred to 34 °C for 90 min while control samples remained at 28 °C. Pollen tubes were stained with 50 µM PO1 (Tocris Bioscience) for the final 30 min of incubation.

PO1 fluorescence was visualized using a Zeiss 880 LSCM using Plan-Apochromat 63x/1.2 NA water objective at 2.4x digital zoom. The 488 nm laser at 0.4% power was used for excitation, with emission collected between 544 and 624 nm. Laser settings were identical for all samples within each experiment. A 1.46 Airy Unit pinhole aperture yielding a 1.4 µm section was utilized and gain at 850. Line profiles of PO1 fluorescence intensity were quantified via a 40 µm long line (50 pixels in width) measured from the tip of each pollen tube in Fiji.

For PO1 staining of pistils, a 100 µm PO1 staining solution was prepared by dissolving 100 nmol PO1 in 20 µL DMSO, which was then diluted 50-fold with MES buffer (10 mm MES, 50 μ m CaCl₂, 5 μM KCl, pH 6.15). Buds that were 1 d prior to anthesis (-1 DPA) were emasculated, and the following day, the pistils were harvested and washed once in the MES buffer. The buffer was removed, and the pistils were stained with the 100 μM PO1 staining solution for 30 min at room temperature in the dark. The PO1 staining solution was removed, and pistils were washed twice with MES buffer. The pistils were imaged under a Zeiss V16 Stereoscope (excitation filter: 559 to 585 nm, emission: 600 to 690 nm) using a Plan-Neofluar objective and a 3.2x zoom. Light levels and exposure time were uniform for each image taken. Representative images were maximum intensity projections taken with 32x to illustrate the fluorescent signal, which is concentrated in the stigma, while images used for quantification were single planes taken at 12.5x. Fluorescence intensity of the stigma was quantified by drawing a region of interest around it in Fiji and measuring its mean gray value.

DPBA staining of pollen tubes and pistils

For DPBA imaging of samples with elongated pollen tubes, harvested pollen was incubated in PGM at 28 °C for 90 min. Pollen tubes were then stained with 2.5 µg/ml DPBA diluted into PGM from a 0.25 mg/mL DPBA (Sigma-Aldrich) stock dissolved in DMSO (with a final 1% DMSO concentration) for the final 30 min of incubation.

DPBA fluorescence was visualized using a Zeiss 880 LSCM using Plan-Apochromat 63x/1.2 NA water objective at 2.4x digital zoom. The 458 nm laser at 4% power was used for excitation, with emission collected between 544 and 624 nm. Laser settings were kept identical for all samples within each experiment. A 2.27 Airy Unit pinhole aperture yielding a 2 µm section was utilized and gain at 850. Line profiles of DPBA fluorescence intensity were quantified via a 40 µm long line (50 pixels in width) measured from the tip of each pollen tube in Fiji.

For DPBA visualization in pistils, buds that were -1 DPA were emasculated, and the following day, the pistils were harvested and washed once in 1x PBS. The PBS was removed, and the pistils were stained with DPBA (2.5 mg/mL DPBA and 0.06% [v/v] Triton X-100 dissolved in 1x PBS) for 20 min at room temperature in the dark. The DPBA staining solution was removed, and pistils were washed twice with 1x PBS. The pistils were imaged under a Zeiss V16 Stereoscope (excitation: 470 nm, emission: 495 to 575 nm) using a Zeiss Plan-Apochromat 5x/0.16 NA objective. Light level and exposure time were uniform for each image taken. Representative images were maximum intensity projections taken with 32x to illustrate the fluorescent signal that is concentrated in the stigma, while images used for quantification were single planes taken at 12.5x. Fluorescence intensity of the stigma regions was quantified by drawing a region of interest around the stigma in Fiji and measuring its mean gray value.

Pollen tube growth through pistil explants

Buds that were -1 DPA were emasculated, and the following day, the pistils were harvested. Pollen from at least 3 flowers of each line was collected as stated previously and pooled together in a microcentrifuge tube. The tube was inverted to collect the pollen onto the cap, and the pollen was used to pollinate the emasculated pistils. The pollinated pistils were placed on a Petri dish with solid 1x MS media (0.8% [w/v] agar, 0.05% [w/v] MES, 1% sucrose, 1 µg/mL thiamine HCl, 0.5 µg/mL pyridoxine HCl, and 0.5 µg/mL nicotinic acid) and incubated for 7 h at 28 °C. Then, pistils were fixed in 3:1 (v/v) ethanol:glacial acetic acid for at least 18 h at room temperature. The fixative was removed, and the pistils were sequentially washed in 70%, 30%, and then 0% ethanol v/v, each for at least 15 min. The pistils were cleared in a solution of 10 N NaOH for at least 4 h, washed in distilled water for at least 10 min, and then stained for at least 12 h in the dark in decolorized aniline blue (0.1% [w/v] aniline blue in 0.1 M K₃PO₄, incubated for 24 h at room temperature in the dark, which leads to loss of blue contaminants but not the fluorochrome that binds callose). After decolorization, the aniline blue solution changes from dark blue to a light yellow color.

Stained pistils were mounted on a glass coverslip in 100% v/v glycerol and then imaged with the 5x objective of a Zeiss 880 LSCM with a Plan-Apochromat 5x/0.16 NA objective (excitation: 405 nm, emission: 416 to 511 nm) and detector gain of 600. Individual images were stitched together using the MosaicJ plugin (Thévenaz and Unser 2007) in Fiji. The number of pollen tubes that penetrated through the stigma was quantified using the Cell Counter plugin in Fiji.

Exogenous chemical treatments

Flavonol chemical complementation was achieved through the addition of quercetin, kaempferol, or myricetin (INDOFINE Chemical) to PGM at final concentrations of 1, 5, 15, or 30 $\mu \rm M$ (diluted from stock solutions of 0.1, 0.5, 1.5, and 3 mm in DMSO). An equivalent volume of DMSO was added to the controls. For VAS2870 treatment, a 50 $\mu \rm M$ stock solution (using diH2O as a solvent) was diluted in PGM to yield a final concentration of 1 $\mu \rm M$, while control samples received an equivalent volume of diH2O. Pollen was resuspended in PGM equilibrated to either 28 or 34 °C containing flavonols or VAS2870 at the indicated concentrations, and germination and tube length were quantified as described above.

Visualization and quantification of DCF fluorescence in pollen grains and pollen tubes

For quantification of ROS during pollen germination, pollen grains were harvested as described above and pollen was allowed to germinate for 10 min in PGM alone at 28 or 34 °C and then 5 $\mu\rm M$ CM-H₂DCFDA (Thermo Fisher), diluted from a stock solution of 500 $\mu\rm M$ in DMSO, was added for another 20 min at 28 or 34 °C. Pollen was then centrifuged, the PGM containing CM-H₂DCFDA was removed and replaced with PGM alone, and the stained pollen was transferred to a microscope slide for imaging.

For DCF imaging of samples with elongated pollen tubes, harvested pollen was incubated at 28 °C for 30 min. Heat-treated samples were then incubated at 34 °C for 90 min while control samples remained at 28 °C. Pollen tubes were then stained with 5 $\mu\rm M$ CM-H₂DCFDA (Thermo Fisher) for 20 min. Pollen was then centrifuged, the PGM containing CM-H₂DCFDA was removed and replaced with PGM alone, and stained pollen tubes were transferred to a microscope slide for imaging.

DCF fluorescence was visualized using a Zeiss 880 LSCM with a Plan-Apochromat 10x/0.45 NA objective using the 488 nm laser and an emission spectrum of 490 to 606 nm. Laser settings were uniform for all samples within each experiment, but for the pollen germination or pollen tube assays, settings were optimized to make sure all samples were below saturating levels of fluorescence. Laser power ranged from 0.9% to 1.5%, and a 1 Airy Unit pinhole aperture yielding a 1.2 μ m section was utilized and gain ranged from 974 to 1,034. The DCF fluorescence intensity was quantified in Fiji, and each experiment was normalized to fluorescence of VF36 at 28 °C.

Measurement of F3H transcript abundance by RT-qPCR

There is conflicting evidence in the literature on whether the 35S promoter is expressed in pollen, so we verified F3H transcript changes in anther tissues. Eyal et al. (1995) showed that a 500 bp 35S promoter was not an optimal promoter for transient expression in pollen. The Maloney construct used the vector pK7WG2, which has a 900 bp region of the 35S promoter, which may have different tissue-specific expression patterns (Maloney et al. 2014). We note that Pro35S:GUS or Pro35S:GFP expression has been detected in tomato floral structures in stable transformants (Koul et al. 2012) and in both strawberry and cotton pollen and anthers (Sunilkumar et al. 2002; de Mesa et al. 2004). Additionally, published evidence suggests that flavonol accumulation in pollen is deposited during pollen development by tapetum cells within the anther (van Eldik et al. 1997; Shi et al. 2021; Xue et al. 2023); therefore, we evaluated F3H expression in anther tissue of VF36, are, are-F3H-T5, and VF36-F3H-T3.

To extract total RNA from anthers, the fully mature pollen grains were removed from anthers by extended vibration, and then anthers were harvested and weighed and were immediately frozen in liquid nitrogen and stored at -80 °C until extraction. Anther samples were homogenized into a fine powder using a bead beater. Following homogenization, total RNA was extracted using QIAGEN RNeasy Plant Mini Kit. After DNase I treatment using the RapidOut DNA Removal Kit (Thermo Scientific), RNA concentration was quantified using a NanoDrop Spectrophotometer (Thermo Scientific). A total of 500 ng of RNA was used for cDNA synthesis in a total volume of 20 μ L, utilizing Super Script II reverse transcriptase. Subsequently, the cDNA underwent treatment with RNase H (Promega). To quantify transcript level of F3H gene, RT-qPCR was performed using gene-specific primer pairs for F3H (PRAM_26184.1) and actin (Solyc03g078400) (the reference gene). Primer sequences used were as follows: F3H: Fw TCTTGGCGATCACGGTCATT, Rv GCAAATGTAATCGGCTCATCCA and Actin: Fw TCTCTGTTGGCCTTGGGATT, Rv CTTCGAGTTG CTCCTGAGGAA. For RT-qPCR, SYBR Green Master Mix (Life Technologies) was used and cDNA was amplified on an Applied Biosystems Real-Time PCR Instrument. The transcript abundance was quantified using a standard curve method using a 2-fold dilution series of templates with amplification of either Actin or F3H with gene-specific primers. F3H transcript abundance was normalized relative to the Actin reference gene, and values are reported relative to VF36 samples. This experiment was performed using a total of 6 biological replicates, and each had 3 technical replicates.

Extraction and quantification of aglycone flavonols in pollen and anthers

For flavonol extractions, pollen was harvested, immediately frozen in liquid nitrogen, and stored at $-80~^\circ\text{C}$ until extraction. For

anthers, pollen grains were removed by extended vibration and the weight was determined before samples were frozen in liquid nitrogen. Pollen samples were resuspended in 300 µL PVS (290 mм sucrose, 1.27 mм Ca(NO₃)₂, 0.16 mм boric acid, 1 mм KNO₃), and the number of live grains in the sample was quantified using a hemocytometer or Countess II Automated Cell Counter (Invitrogen). Pollen was recovered by centrifugation, and the PVS was removed and replaced with 300 µL extraction buffer (containing 500 nm formononetin internal standard that was dissolved in acetone). Anther samples were homogenized into a fine powder using a bead beater, after which 300 µL extraction buffer was added to thoroughly mix the powder.

Pollen and anther samples were incubated in the extraction buffer at 4 °C for 20 min. A volume of 2 N HCl equal to the volume of the extraction buffer was added to the samples, and they were incubated at 75 °C for 45 min to release aglycone flavonols. An equal volume of ethyl acetate (Optima Grade, Fisher) was added to the aglycone flavonols and shaken for 5 min before microcentrifugation at $17,000 \times g$ for 10 min. The top organic (ethyl acetate) phase was isolated, and the ethyl acetate phase separation was repeated. The collected organic phases were pooled. Samples were dried by airflow using a mini-vap evaporator (Supelco Inc) and resuspended in 50 µL of acetonitrile before LC-MS analysis.

Following resuspension in acetonitrile, samples were analyzed on a TSQ Triple Quadrupole Mass Spectrometer with an electrospray ionization source, coupled to a Thermo Accela 1250 pump and autosampler (Thermo Fisher). For analysis of flavonol extracts, 10 µL of each sample was injected on a Luna 150 x 3 mm C18 column with a SecurityGuard precolumn with a solvent of water:acetonitrile, both containing 0.1% (v/v) formic acid. The solvent gradient was 90% water (v/v):10% acetonitrile (v/v) to 10% water (v/v):90% acetonitrile (v/v) in a time span of 18.5 min. From 18.5 to 20 min, the gradient moved from 10% water (v/v):90% acetonitrile (v/v) back to 90% water (v/v):10% acetonitrile (v/v) and held at those concentrations for another 2 min to recondition the column. Quantification of flavonols was found by comparing the MS1 peak area data, quantified in Thermo Xcalibur, to standard curves, with concentrations of $1 \mu M$, 500 nm, 250 nm, 125 nm, 62.5 nm, 10 nm, 5 nm, and 1 nm, generated using pure standards of naringenin, quercetin, kaempferol, and myricetin (INDOFINE Chemical). Total flavonol level was calculated by averaging the total flavonol value of each sample. MS2 fragmentation spectra were collected to confirm flavonol identity/structure. Fragmentation was induced using 24- to 41-kV collision-induced dissociation, optimized for each compound. MS2 spectra of each flavonol in plant extracts were compared with the MS2 spectra of the standards described above. The flavonol content in each pollen sample was normalized to the number of live grains in the sample and reported in units of fmoles/10,000 grains, while the flavonol levels in anthers were reported relative to mg fresh weight.

Pollen sample preparation and RNA isolation for sequencing

Pollen was harvested as described above from VF36, are, and VF36-F3H-T3 using 4 to 7 flowers of VF36 and VF36-T3 and 3 times as many flowers from are to result in similar yields of pollen across genotypes. For the 15- and 30-min timepoints, pollen was resuspended in 100 µL PGM equilibrated at 28 °C. For each genotype, $20 \,\mu L$ of pollen suspension was then transferred to 4 separate 1.5-mL microcentrifuge tubes containing 980 µL of PGM equilibrated at either 28 or 34 °C (15- and 30-min timepoints at 28 °C and matching timepoints at 34 °C) and incubated in water baths set to the corresponding temperatures. An additional 5 µL from each pollen suspension was also transferred to two 24-well plates. equilibrated at 28 or 34 °C, to be imaged live as described earlier for the evaluation of pollen germination. For each replicate, we verified that the impaired pollen performance of are and robust pollen performance of VF36-T3 were evident as judged by pollen tube integrity and growth. Pollen was incubated at either 28 or 34 °C for 15 min, and then samples for the corresponding timepoint were removed and pelleted by centrifugation at $10,000 \times g$ for 1 min. Supernatant PGM was removed from each tube until only the pellet remained and pollen samples were flash frozen in liquid nitrogen. The same procedure was repeated for the 30-min timepoint after the completion of incubation.

For the 45- and 75-min timepoints, pollen was resuspended in 100 μL PGM equilibrated to 28 °C. For each genotype, 20 μL of pollen suspension was then transferred to 4 separate 1.5-mL microcentrifuge tubes containing 980 µL of PGM that were all equilibrated to 28 °C and incubated in the 28 °C water bath for 30 min. An additional 5 μ L from each pollen suspension was also transferred to two 24-well plates that were equilibrated to 28 °C, to be germinated for 30 min. After 30-min incubation at 28 °C, 2 microcentrifuge tubes from each genotype were transferred to the 34 °C water bath to be incubated for an additional 45 or 75 min while the other 2 tubes remained at 28 °C. One 24-well plate was also transferred to 34 °C to be imaged live as described earlier for the evaluation of pollen tube elongation. Pollen was incubated at either 28 or 34 °C for 45 additional minutes (75 min total growth), and then samples for the corresponding timepoint were removed and pelleted by centrifugation at 10,000 x q for 1 min. PGM was removed from each tube until only the pellet remained and pollen samples were flash frozen in liquid nitrogen. The same procedure was repeated for the 75-min timepoint (105 min total growth) after the completion of incubation.

Pellets were pulverized using sterile micropestles in liquid nitrogen (Thermo Fisher), and RNA isolation was completed in accordance with the QIAGEN Plant RNeasy Kit Protocol (QIAGEN). DNA was removed via off-column DNase treatment with the RapidOut DNA Removal Kit (Thermo Scientific). Concentrations for each sample were quantified via a NanoDrop Spectrophotometer (Thermo Fisher) after initial RNA isolation and again following DNase treatment. Each sample contained at least 1.5 µg of RNA. GENEWIZ, LLC (Azenta Life Sciences) completed paired-end, strand-specific RNA sequencing through utilization of the Illumina HiSeq platform.

Analysis of RNA-seq samples

All analysis and data processing code, along with documentation and RNA-seq "counts" data files, are available from the project "git" repository (https://bitbucket.org/hotpollen/flavonoidrnaseq). The raw read files are available in the NCBI: Sequencing Read Archive (SRA) under the project name SRP460750. The RNA sequencing data were processed through the nf-core/maseq pipeline version 3.4 (Ewels et al. 2020). Sequences were aligned to the 2 most recently published tomato genome assemblies and annotation sets, designated SL4/S_lycopersicum_Sep_2019 and SL5/ S_lycopersicum_Jun_2022 (Zhou et al. 2022) using the Salmon/ STAR option settings (Dobin et al. 2012) for the nf-core/maseq pipeline. All gene IDs utilized in the text or in figures refer to the SL5 version of the tomato genome. The pipeline produced RNA-seq to genome assembly alignment files, one per input library. To enable visual detection of differential expression across samples, we further processed the alignment files using the "bamCoverage" function from deepTools, a suite of commandline programs for processing and analyzing RNA-seq and other high-throughput sequence data sets (Ramírez et al. 2016). This produced scaled coverage graphs reporting the number of aligned RNA-seq fragments per genomic base pair position, scaled by library sequencing depth, allowing visual comparison of expression levels across samples. To enable visualization and assessment of splicing patterns, FindJunctions (https://bitbucket.org/lorainelab/ findjunctions/) was used to create "BED" format files reporting the genomic coordinates of introns inferred from the data and the number of alignments supporting the discovered intron. The RNA-seg alignment, coverage graph, and junction files were deployed to an IGB Quickload site for visualization in the Integrated Genome Browser (IGB) (Freese et al. 2016). Code used to create the IGB Quickload site, along with instructions on how to use IGB to view and explore the data, are available from https://bitbucket. org/hotpollen/genome-browser-visualization.

In addition to RNA-seq alignment files, the nf-core/maseq pipeline produced a gene expression counts table reporting the number of RNA-seq fragments observed per gene, per sample, with each column representing a different experimental sample consisting of different time, temperature, genotype, and replicate. The time course consisted of 2 timepoints in the germination phase (15 and 30 min), and 2 timepoints in the pollen tube elongation phase (45 and 75 min of heat treatment for a total of 75 and 105 min of growth, respectively) at 28 or 34 °C. Genotypes sequenced were VF36, VF36-F3H-T3, or are. The gene expression counts tables were provided as inputs to differential expression analysis code that used DESeq2 (Love et al. 2014) to identify DEGs either between elevated temperature treatment (34 °C) and optimal (control) samples germinated at 28 °C within genotype and length of growth or between genotypes at each temperature and timepoint. The DESeq2 model internally corrects for library size and sequencing depth. Thus, preprocessing the counts file by transforming or normalizing count-based expression values was not necessary as input. However, for visualization and validation of differential expression results, we created scaled expression data files using "counts per million" units, by dividing counts values by the total number of aligned fragments and multiplying by 1,000,000. The original counts files and derived scaled counts files are available in the code repository, along with the code used to generate them.

For exploratory visualization and clustering analysis, PCA and volcano plots were created using DESeq library function plotPCA (https://www.rdocumentation.org/packages/DESeq2/versions/1. 12.3/topics/plotPCA), plotting functions from the gaplot package (https://ggplot2.tidyverse.org/), and functions from the Enhanced Volcano plot package (https://github.com/kevinblighe/Enhanced Volcano). Volcano plots were produced using the DESeq2 output comparing samples treated at 28 °C to those treated at 34 °C for each timepoint to explore the DEGs that are impacted by heat stress. To facilitate exploration and validation of results, RShiny apps were created that show bar plots summarizing gene expression values across all samples.

Statistics

All statistical analyses of growth and fluorescence were performed using GraphPad Prism 9 with a 2-way ANOVA followed by a Tukey post hoc test. For the quantification of flavonol abundance by LC-MS, a 1-way ANOVA was used followed by a Dunnett's post hoc test, except as noted where t tests were used to compare 2 samples. For the analysis of pollen tube penetration through the stigma, a 1-way ANOVA was used followed by a Tukey

post hoc test. A complete set of results from all ANOVAs are reported in Supplementary Data Set 6, where variables, parameters, degrees of freedom, and test statistics are reported. Comparisons of DPBA and PO1 fluorescence levels between VF36 and *are* stigmas were accomplished by a Student's t test.

Accession numbers

The tomato F3H gene is Solyc02g083860 or PRAM_26184.1 in the 4th and 5th versions of the tomato genome, respectively. The accession numbers using the 4th version of the tomato genome annotation reported in Fig. 14 are Solyc06G000727, Solyc12G002286, Solyc11G002443, Solyc01G003506, Solyc08G002253, Solyc06G002092, Solyc03G002803, Solyc06G002439, Solyc01G00268, Solyc07G002746, Solyc10G002699, Solyc08G002151, Solyc03G000301, Solyc04G002402, Solyc01G002128, Solyc03G003038, Solyc04G000427, PRAM_26312, Solyc01G003823, Solyc11G002064, Solyc10G002281, Solyc12G000755, Solyc01G000420, Solyc07G002080, Solyc01G003554, Solyc01G003745, Solyc09G000013, Solyc03G001922, Solyc08G002201, Solyc12G002528, Solyc11G001539, Solyc01G001877, Solyc08G002146, Solyc07G001653, Solyc05G000603, and Solyc04G001597, and gene IDs for all other DEGs are reported in Supplementary Data Sets 1 to 5.

Acknowledgments

The authors would like to thank the current and past members of the Muday lab (especially Dr. Joëlle Mühlemann and Dr. Gregory Maloney) and the Genomics of Thermotolerance in Tomato (GTTR) group for their suggestions and editorial input and Nina Bravo Chan for assistance with analysis of the pollen tube growth through pistils.

Author contributions

A.E.P., A.M.D., E.Y.W., M.H., and G.K.M. designed experiments. A.E.P., A.M.D., M.F.A., M.H., S.L.H., C.M.R., and E.Y.W. performed research and analyzed data. M.G.K., M.D., R.W.R., A.E.L., and J.B.P. performed computational analysis and/or wrote sections explaining the RNA sequencing data or PaLD analysis. A.E.P., A.M.D., E.Y.W., and G.K.M. wrote and edited the paper, and all authors provided editorial suggestions.

Supplementary data

The following materials are available in the online version of this article.

Supplementary Figure S1. Pollen viability immediately after harvesting is impaired in *are*.

Supplementary Figure S2. Increased transcript abundance of F3H gene in anthers of VF36-T3 compared to VF36.

Supplementary Figure S3. Separate transformants of either *are* or VF36 with the Pro35S:F3H gene reveal similar increases in pollen germination.

Supplementary Figure S4. Chemical complementation with quercetin and myricetin protects pollen germination from the negative effects of heat exposure.

Supplementary Figure S5. Workflow for pollen sample preparation for transcriptome analysis using RNA-seq.

Supplementary Figure S6. All *are* samples in RNA-seq analysis contain a point mutation in the F3H gene (PRAM_26184.1).

Supplementary Figure S7. Volcano plots for 15-min samples for *are*, VF36, and VF36-T3.

Supplementary Figure S8. Volcano plots for 30-min samples for *are*, VF36, and VF36-T3.

Supplementary Figure S9. Volcano plots for 45-min samples for are, VF36, and VF36-T3.

Supplementary Figure S10. The heat-dependent DEGs for VF36. **Supplementary Figure S11.** The heat-dependent DEGs for are. Supplementary Figure S12. The heat-dependent DEGs for VF36-T3.

Supplementary Figure S13. DEGs between are and VF36 at every timepoint and temperature.

Supplementary Figure S14. Morphological differences between viable and nonviable pollen grains.

Supplementary Table S1. Quantification of flavonol levels in anthers and pollen grains.

Supplementary Table S2. Scaled read count for expressed genes in pollen.

Supplementary Table S3. Number of DE transcripts between are and VF36.

Supplementary Data Set 1. VF36 control vs temperature DEGs. **Supplementary Data Set 2.** are control vs temperature DEGs. Supplementary Data Set 3. VF36-T3 control vs temperature

Supplementary Data Set 5. are vs VF36 control DEGs. Supplementary Data Set 4. VF36-are PaLD community groups. Supplementary Data Set 6. Statistical analysis.

Funding

This project was supported by the United States Department of Agriculture-National Institute of Food and Agriculture (2020-67013-30907 to G.K.M.), National Science Foundation Plant Genome Research Program (IOS 1939255 to G.K.M., J.B.P., and A.E.L.), National Institute of Health National Institute of General Medical Sciences (5R35GM139609 to A.E.L.), an National Institute of Health T32 (GM127261 fellowship supported A.E.P.), and a Wake Forest University Center for Molecular Signaling Summer Research Fellowship to E.Y.W.

Conflict of interest statement. None declared.

Data availability

The transcriptomic data underlying this article are available in NCBI: Sequencing Read Archive (SRA), and can be accessed with under the project name SRP460750. Other data underlying this article will be shared on reasonable request to the corresponding author.

References

- Agati G, Azzarello E, Pollastri S, Tattini M. Flavonoids as antioxidants in plants: location and functional significance. Plant Sci. 2012:196: 67-76. https://doi.org/10.1016/j.plantsci.2012.07.014
- Ali MF, Muday GK. Reactive oxygen species are signaling molecules that modulate plant reproduction. Plant Cell Environ. 2024:47(5): 1592-1605. https://doi.org/10.1111/pce.14837
- Alseekh S, Perez de Souza L, Benina M, Fernie AR. The style and substance of plant flavonoid decoration; towards defining both structure and function. Phytochemistry. 2020:174:112347. https://doi. org/10.1016/j.phytochem.2020.112347
- Begcy K, Nosenko T, Zhou L-Z, Fragner L, Weckwerth W, Dresselhaus T. Male sterility in maize after transient heat stress during the tetrad stage of pollen development. Plant Physiol. 2019:181(2): 683-700. https://doi.org/10.1104/pp.19.00707
- Berenhaut KS, Moore KE, Melvin RL. A social perspective on perceived distances reveals deep community structure. Proc Natl

- Acad Sci U S A. 2022:119(4):e2003634119 https://doi.org/10.1073/ pnas.2003634119
- Bita CE, Zenoni S, Vriezen WH, Mariani C, Pezzotti M, Gerats T. Temperature stress differentially modulates transcription in meiotic anthers of heat-tolerant and heat-sensitive tomato plants. BMC Genomics. 2011:12(1):384. https://doi.org/10.1186/ 1471-2164-12-384
- Chapman JM, Muday GK. Flavonols modulate lateral root emergence by scavenging reactive oxygen species in Arabidopsis thaliana. J Biol Chem. 2021:296:100222. https://doi.org/10.1074/jbc.RA120.014543
- Chapman JM, Muhlemann JK, Gayomba SR, Muday GK. RBOH-dependent ROS synthesis and ROS scavenging by plant specialized metabolites to modulate plant development and stress responses. Chem Res Toxicol. 2019:32(3):370-396. https:// doi.org/10.1021/acs.chemrestox.9b00028
- Chaturvedi P, Wiese AJ, Ghatak A, Záveská Drábková L, Weckwerth W, Honys D. Heat stress response mechanisms in pollen development. New Phytol. 2021:231(2):571-585. https://doi.org/10.1111/ nph.17380
- Considine MJ, Foyer CH. Oxygen and reactive oxygen speciesdependent regulation of plant growth and development. Plant Physiol. 2021:186(1):79–92. https://doi.org/10.1093/plphys/kiaa077
- Dai X, Han H, Huang W, Zhao L, Song M, Cao X, Liu C, Niu X, Lang Z, Ma C, et al. Generating novel male sterile tomatoes by editing respiratory burst oxidase homolog genes. Front Plant Sci. 2021:12: 817101. https://doi.org/10.3389/fpls.2021.817101
- Daryanavard H, Postiglione AE, Mühlemann JK, Muday GK. Flavonols modulate plant development, signaling, and stress responses. Curr Opin Plant Biol. 2023:72:102350. https://doi.org/10.1016/j.pbi. 2023.102350
- de Mesa MC, Santiago-Doménech N, Pliego-Alfaro F, Quesada MA, Mercado JA. The CaMV 35S promoter is highly active on floral organs and pollen of transgenic strawberry plants. Plant Cell Rep. 2004:23(1–2):32–38. https://doi.org/10.1007/s00299-004-0776-0
- De Storme N, Geelen D. The impact of environmental stress on male reproductive development in plants: biological processes and molecular mechanisms. Plant Cell Environ. 2014:37(1):1-18. https://doi.org/10.1111/pce.12142
- Dinar M, Rudich J. Effect of heat stress on assimilate partitioning in tomato. Ann Bot. 1985:56(2):239-248. https://doi.org/10.1093/ oxfordjournals.aob.a087008
- Dobin A, Davis CA, Schlesinger F, Drenkow J, Zaleski C, Jha S, Batut P, Chaisson M, Gingeras TR. STAR: ultrafast universal RNA-seq aligner. Bioinformatics. 2012:29(1):15-21. https://doi.org/10.1093/ bioinformatics/bts635
- Ewels PA, Peltzer A, Fillinger S, Patel H, Alneberg J, Wilm A, Garcia MU, Di Tommaso P, Nahnsen S. The nf-core framework for community-curated bioinformatics pipelines. Nat Biotechnol. 2020:38(3):276-278. https://doi.org/10.1038/s41587-020-0439-x
- Eyal Y, Curie C, McCormick S. Pollen specificity elements reside in 30 bp of the proximal promoters of two pollen-expressed genes. Plant Cell. 1995:7(3):373–384. https://doi.org/10.1105/tpc.7.3.373
- Fahad S, Bajwa AA, Nazir U, Anjum SA, Farooq A, Zohaib A, Sadia S, Nasim W, Adkins S, Saud S, et al. Crop production under drought and heat stress: plant responses and management options. Front Plant Sci. 2017:8:1147. https://doi.org/10.3389/fpls.2017.01147
- Falcone Ferreyra ML, Rius SP, Casati P. Flavonoids: biosynthesis, biological functions, and biotechnological applications. Front Plant Sci. 2012:3:222. https://doi.org/10.3389/fpls.2012.00222
- Firon N, Shaked R, Peet MM, Pharr DM, Zamski E, Rosenfeld K, Althan L, Pressman E. Pollen grains of heat tolerant tomato cultivars retain higher carbohydrate concentration under heat stress

- conditions. Sci Hortic. 2006:109(3):212–217. https://doi.org/10.1016/j.scienta.2006.03.007
- Frank G, Pressman E, Ophir R, Althan L, Shaked R, Freedman M, Shen S, Firon N. Transcriptional profiling of maturing tomato (Solanum lycopersicum L.) microspores reveals the involvement of heat shock proteins, ROS scavengers, hormones, and sugars in the heat stress response. *J Exp Bot.* 2009:60(13):3891–3908. https://doi.org/10.1093/jxb/erp234
- Freese NH, Norris DC, Loraine AE. Integrated genome browser: visual analytics platform for genomics. Bioinformatics. 2016:32 (14):2089–2095. https://doi.org/10.1093/bioinformatics/btw069
- Garrido Ruiz D, Sandoval-Perez A, Rangarajan AV, Gunderson EL, Jacobson MP. Cysteine oxidation in proteins: structure, biophysics, and simulation. *Biochemistry*. 2022:61(20):2165–2176. https://doi.org/10.1021/acs.biochem.2c00349
- Gayomba SR, Muday GK. Flavonols regulate root hair development by modulating accumulation of reactive oxygen species in the root epidermis. *Development*. 2020:147(8):dev185819. https://doi.org/10.1242/dev.185819
- Gayomba SR, Watkins JM, Muday GK. Flavonols regulate plant growth and development through regulation of auxin transport and cellular redox status. In: Yoshidaessor K, Director VCR, Quideauessor S, editors. Recent advances in polyphenol research. Hoboken, New Jersey, U.S.: John Wiley & Sons, Ltd; 2017. p. 143–170. https://doi.org/10.1002/9781118883303.ch7
- Gong W, Oubounyt M, Baumbach J, Dresselhaus T. Heatstress-induced ROS in maize silks cause late pollen tube growth arrest and sterility. iScience. 2024:27(7):110081. https://doi.org/ 10.1016/j.isci.2024.110081
- Gonzali S, Perata P. Anthocyanins from purple tomatoes as novel antioxidants to promote human health. *Antioxidants (Basel)*. 2020:9(10):1017. https://doi.org/10.3390/antiox9101017
- Groenenboom M, Gomez-Roldan V, Stigter H, Astola L, van Daelen R, Beekwilder J, Bovy A, Hall R, Molenaar J. The flavonoid pathway in tomato seedlings: transcript abundance and the modeling of metabolite dynamics. PLoS One. 2013:8(7):e68960. https://doi.org/10.1371/journal.pone.0068960
- Jahan MS, Shu S, Wang Y, Chen Z, He M, Tao M, Sun J, Guo S. Melatonin alleviates heat-induced damage of tomato seedlings by balancing redox homeostasis and modulating polyamine and nitric oxide biosynthesis. BMC Plant Biol. 2019:19(1):414. https://doi.org/10.1186/s12870-019-1992-7
- Jiménez-Quesada MJ, Traverso JÁ, Alché JdD. NADPH oxidasedependent superoxide production in plant reproductive tissues. Front Plant Sci. 2016:7:359–359. https://doi.org/10.3389/fpls.2016. 00359
- Jimenez-Quesada MJ, Traverso JA, Potocký M, Žárský V, Alché JdD. Generation of superoxide by OeRbohH, a NADPH oxidase activity during olive (Olea europaea L.) pollen development and germination. Front Plant Sci. 2019:10:1149. https://doi.org/10.3389/fpls. 2019.01149
- Johnson MA, Harper JF, Palanivelu R. A fruitful journey: pollen tube navigation from germination to fertilization. *Annu Rev Plant Biol.* 2019:70(1):809–837. https://doi.org/10.1146/annurev-arplant-050 718-100133
- Kaya H, Nakajima R, Iwano M, Kanaoka MM, Kimura S, Takeda S, Kawarazaki T, Senzaki E, Hamamura Y, Higashiyama T, et al. Ca2+-activated reactive oxygen species production by Arabidopsis RbohH and RbohJ is essential for proper pollen tube tip growth. *Plant Cell*. 2014:26(3):1069–1080. https://doi.org/10.1105/tpc.113.120642
- Khoury MG, Berenhaut KS, Moore KE, Allen EE, Harkey AF, Mühlemann JK, Craven CN, Xu J, Jain SS, John DJ, et al. Informative

- community structure revealed using Arabidopsis time series transcriptome data via partitioned local depth. in silico Plants. 2023:6:diad018. https://doi.org/10.1093/insilicoplants/diad018
- Koul B, Yadav R, Sanyal I, Sawant S, Sharma V, Amla DV. Cis-acting motifs in artificially synthesized expression cassette leads to enhanced transgene expression in tomato (Solanum lycopersicum L.). Plant Physiol Biochem. 2012:61:131–141. https://doi.org/10.1016/j. plaphy.2012.09.014
- Kovinich N, Kayanja G, Chanoca A, Riedl K, Otegui MS, Grotewold E. Not all anthocyanins are born equal: distinct patterns induced by stress in Arabidopsis. Planta. 2014:240(5):931–940. https://doi.org/ 10.1007/s00425-014-2079-1
- Ku YS, Ng MS, Cheng SS, Lo AW, Xiao Z, Shin TS, Chung G, Lam HM. Understanding the composition, biosynthesis, accumulation and transport of flavonoids in crops for the promotion of crops as healthy sources of flavonoids for human consumption. Nutrients. 2020:12(6):1717. https://doi.org/10.3390/nu12061717
- Lee JY, Kim H, Gasparrini A, Armstrong B, Bell ML, Sera F, Lavigne E, Abrutzky R, Tong S, Coelho MSZS, et al. Predicted temperature-increase-induced global health burden and its regional variability. Environ Int. 2019:131:105027. https://doi.org/10.1016/j.envint.2019.105027
- Lewis DR, Ramirez MV, Miller ND, Vallabhaneni P, Ray WK, Helm RF, Winkel BS, Muday GK. Auxin and ethylene induce flavonol accumulation through distinct transcriptional networks. *Plant Physiol.* 2011:156(1):144–164. https://doi.org/10.1104/pp.111.172502
- Lohani N, Singh MB, Bhalla PL. High temperature susceptibility of sexual reproduction in crop plants. *J Exp Bot*. 2019:71(2):555–568. https://doi.org/10.1093/jxb/erz426
- Love MI, Huber W, Anders S. Moderated estimation of fold change and dispersion for RNA-seq data with DESeq2. *Genome Biol.* 2014:15(12):550. https://doi.org/10.1186/s13059-014-0550-8
- Maloney GS, DiNapoli KT, Muday GK. The anthocyanin reduced tomato mutant demonstrates the role of flavonols in tomato lateral root and root hair development. Plant Physiol. 2014: 166(2):614–631. https://doi.org/10.1104/pp.114.240507
- Mangano S, Denita-Juarez SP, Choi HS, Marzol E, Hwang Y, Ranocha P, Velasquez SM, Borassi C, Barberini ML, Aptekmann AA, et al. Molecular link between auxin and ROS-mediated polar growth. Proc Natl Acad Sci U S A. 2017:114(20):5289–5294. https://doi.org/10.1073/pnas.1701536114
- Martin RE, Postiglione AE, Muday GK. Reactive oxygen species function as signaling molecules in controlling plant development and hormonal responses. *Curr Opin Plant Biol.* 2022:69:102293. https://doi.org/10.1016/j.pbi.2022.102293
- Mittler R. Oxidative stress, antioxidants and stress tolerance. Trends Plant Sci. 2002:7(9):405–410. https://doi.org/10.1016/S1360-1385(02)02312-9
- Mo Y, Nagel C, Taylor LP. Biochemical complementation of chalcone synthase mutants defines a role for flavonols in functional pollen. Proc Natl Acad Sci U S A. 1992:89(15):7213–7217. https://doi.org/10. 1073/pnas.89.15.7213
- Møller IM, Jensen PE, Hansson A. Oxidative modifications to cellular components in plants. Annu Rev Plant Biol. 2007:58(1):459–481. https://doi.org/10.1146/annurev.arplant.58.032806.103946
- Muhlemann JK, Younts TLB, Muday GK. Flavonols control pollen tube growth and integrity by regulating ROS homeostasis during high-temperature stress. Proc Natl Acad Sci U S A. 2018:115(15): E11188–E11197. https://doi.org/10.1073/pnas.1811492115
- Paupière MJ, Müller F, Li H, Rieu I, Tikunov YM, Visser RGF, Bovy AG. Untargeted metabolomic analysis of tomato pollen development and heat stress response. Plant Reprod. 2017:30(2):81–94. https://doi.org/10.1007/s00497-017-0301-6

- Paupière MJ, Van Heusden AW, Bovy AG. The metabolic basis of pollen thermo-tolerance: perspectives for breeding. Metabolites. 2014:4(4):889-920. https://doi.org/10.3390/metabo4040889
- Pollak PE, Vogt T, Mo Y, Taylor LP. Chalcone synthase and flavonol accumulation in stigmas and anthers of Petunia hybrida. Plant Physiol. 1993:102(3):925–932. https://doi.org/10.1104/pp.102.3.925
- Postiglione AE, Muday GK. Abscisic acid increases hydrogen peroxide in mitochondria to facilitate stomatal closure. Plant Physiol. 2022:192(1):469-487. https://doi.org/10.1093/plphys/kiac601
- Potocký M, Jones MA, Bezvoda R, Smirnoff N, Žárský V. Reactive oxygen species produced by NADPH oxidase are involved in pollen tube growth. New Phytol. 2007:174(4):742-751. https://doi.org/10. 1111/j.1469-8137.2007.02042.x
- Pourcel L, Bohórquez-Restrepo A, Irani NG, Grotewold E. Anthocyanin biosynthesis, regulation, and transport: new insights from model species. Recent advances in polyphenol research. Hoboken, New Jersey, U.S. 2012. p. 143-160. https://doi.org/10. 1002/9781118299753.ch6.
- Pressman E, Peet MM, Pharr DM. The effect of heat stress on tomato pollen characteristics is associated with changes in carbohydrate concentration in the developing anthers. Ann Bot. 2002:90(5): 631-636. https://doi.org/10.1093/aob/mcf240
- Raftery AE, Zimmer A, Frierson DMW, Startz R, Liu P. Less than 2 °C warming by 2100 unlikely. Nat Clim Chang. 2017:7(9):637-641. https://doi.org/10.1038/nclimate3352
- Raja MM, Vijayalakshmi G, Naik ML, Basha PO, Sergeant K, Hausman JF, Khan PSSV. Pollen development and function under heat stress: from effects to responses. Acta Physiol Plant. 2019:41(4): 47. https://doi.org/10.1007/s11738-019-2835-8
- Ramírez F, Ryan DP, Grüning B, Bhardwaj V, Kilpert F, Richter AS, Heyne S, Dündar F, Manke T. deepTools2: a next generation web server for deep-sequencing data analysis. Nucleic Acids Res. 2016:44(W1):W160-W165. https://doi.org/10.1093/nar/gkw257
- Reis J, Massari M, Marchese S, Ceccon M, Aalbers FS, Corana F, Valente S, Mai A, Magnani F, Mattevi A. A closer look into NADPH oxidase inhibitors: validation and insight into their mechanism of action. Redox Biol. 2020:32:101466. https://doi.org/ 10.1016/j.redox.2020.101466
- Rieu I, Twell D, Firon N. Pollen development at high temperature: from acclimation to collapse. Plant Physiol. 2017:173(4): 1967-1976. https://doi.org/10.1104/pp.16.01644
- Rutley N, Miller G, Wang F, Harper JF, Miller G, Lieberman-Lazarovich M. Enhanced reproductive thermotolerance of the tomato high pigment 2 mutant is associated with increased accumulation of flavonols in pollen. Front Plant Sci. 2021:12:672368. https://doi.org/10.3389/fpls.2021.672368
- Saslowsky DE, Warek U, Winkel BSJ. Nuclear localization of flavonoid enzymes in Arabidopsis. J Biol Chem. 2005:280(25):23735-23740. https://doi.org/10.1074/jbc.M413506200
- Sato S, Kamiyama M, Iwata T, Makita N, Furukawa H, Ikeda H. Moderate increase of mean daily temperature adversely affects fruit set of Lycopersicon esculentum by disrupting specific physiological processes in male reproductive development. Ann Bot. 2006:97(5):731-738. https://doi.org/10.1093/aob/mcl037
- Schijlen EGWM, de Vos CHR, Martens S, Jonker HH, Rosin FM, Molthoff JW, Tikunov YM, Angenent GC, van Tunen AJ, Bovy AG. RNA interference silencing of chalcone synthase, the first step in the flavonoid biosynthesis pathway, leads to parthenocarpic tomato fruits. Plant Physiol. 2007:144(3):1520-1530. https://doi.org/10.1104/pp.107.100305
- Shi Y, Jiang X, Chen L, Li WW, Lai S, Fu Z, Liu Y, Qian Y, Gao L, Xia T. Functional analyses of flavonol synthase genes from Camellia

- sinensis reveal their roles in anther development. Front Plant Sci. 2021:12:753131. https://doi.org/10.3389/fpls.2021.753131
- Speranza A, Crinelli R, Scoccianti V, Geitmann A. Reactive oxygen species are involved in pollen tube initiation in kiwifruit. Plant Biol (Stuttg). 2012:14(1):64-76. https://doi.org/10.1111/j.1438-86 77.2011.00479.x
- Sunilkumar G, Mohr L, Lopata-Finch E, Emani C, Rathore KS. Developmental and tissue-specific expression of CaMV 35S promoter in cotton as revealed by GFP. Plant Mol Biol. 2002:50(3): 463-479. https://doi.org/10.1023/A:1019832123444
- Thévenaz P, Unser M. User-friendly semiautomated assembly of accurate image mosaics in microscopy. Microsc Res Tech. 2007:70(2): 135-146. https://doi.org/10.1002/jemt.20393
- Torun H. Time-course analysis of salicylic acid effects on ROS regulation and antioxidant defense in roots of hulled and hulless barley under combined stress of drought, heat and salinity. Physiol Plant. 2019:165(2):169-182. https://doi.org/10.1111/ppl.12798
- van Eldik GJ, Reijnen WH, Ruiter RK, van Herpen MM, Schrauwen JA, Wullems GJ. Regulation of flavonol biosynthesis during anther and pistil development, and during pollen tube growth in Solanum tuberosum. Plant J. 1997:11(1):105-113. https://doi.org/10. 1046/j.1365-313X.1997.11010105.x
- Wang L, Lam PY, Lui ACW, Zhu F-Y, Chen M-X, Liu H, Zhang J, Lo C. Flavonoids are indispensable for complete male fertility in rice. J Exp Bot. 2020:71(16):4715-4728. https://doi.org/10.1093/jxb/
- Watkins JM, Chapman JM, Muday GK. Abscisic acid-induced reactive oxygen species are modulated by flavonols to control stomata aperture. Plant Physiol. 2017:175(4):1807-1825. https://doi.org/10. 1104/pp.17.01010
- Watkins JM, Hechler PJ, Muday GK. Ethylene-induced flavonol accumulation in guard cells suppresses reactive oxygen species and moderates stomatal aperture. Plant Physiol. 2014:164(4): 1707-1717. https://doi.org/10.1104/pp.113.233528
- Wu W, Shah F, Duncan RW, Ma BL. Grain yield, root growth habit and lodging of eight oilseed rape genotypes in response to a short period of heat stress during flowering. Agric For Meteorol. 2020:287: 107954. https://doi.org/10.1016/j.agrformet.2020.107954
- Xu J, Wolters-Arts M, Mariani C, Huber H, Rieu I. Heat stress affects vegetative and reproductive performance and trait correlations in tomato (Solanum lycopersicum). Euphytica. 2017:213(7):156. https://doi.org/10.1007/s10681-017-1949-6
- Xue J-S, Qiu S, Jia X-L, Shen S-Y, Shen C-W, Wang S, Xu P, Tong Q, Lou Y-X, Yang N-Y, et al. Stepwise changes in flavonoids in spores/pollen contributed to terrestrial adaptation of plants. Plant Physiol. 2023:193(1):627-642. https://doi.org/10.1093/plphys/kiad313
- Yoder JI, Belzile F, Tong Y, Goldsbrough A. Visual markers for tomato derived from the anthocyanin biosynthetic pathway. Euphytica. 1994:79(3):163-167. https://doi.org/10.1007/BF00022514
- Yun B-W, Feechan A, Yin M, Saidi NBB, Le Bihan T, Yu M, Moore JW, Kang J-G, Kwon E, Spoel SH, et al. S-Nitrosylation of NADPH oxidase regulates cell death in plant immunity. Nature. 2011:478-(7368):264-268. https://doi.org/10.1038/nature10427
- Zhang D, Wengier D, Shuai B, Gui CP, Muschietti J, McCormick S, Tang WH. The pollen receptor kinase LePRK2 mediates growthpromoting signals and positively regulates pollen germination and tube growth. Plant Physiol. 2008:148(3):1368-1379. https:// doi.org/10.1104/pp.108.124420
- Zhou Y, Zhang Z, Bao Z, Li H, Lyu Y, Zan Y, Wu Y, Cheng L, Fang Y, Wu K, et al. Graph pangenome captures missing heritability and empowers tomato breeding. Nature. 2022:606(7914): 527-534. https://doi.org/10.1038/s41586-022-04808-9